



Combined effects of treated domestic wastewater, fly ash, and calcium nitrite toward concrete sustainability

Abdelrahman Abushanab, Wael Alnahhal*

Department of Civil and Architectural Engineering, College of Engineering, Qatar University, Doha, Qatar

ARTICLE INFO

Keywords:

Sustainable concrete
Treated wastewater
Class F fly ash
Corrosion inhibitor
Durability
Scanning electron microscopy

ABSTRACT

The drastic increase in freshwater and ordinary Portland cement (OPC) consumption poses severe environmental and economic challenges worldwide. This study; therefore, explores the mechanical and durability properties of concrete incorporating treated domestic wastewater (TWW), class F fly ash (FA), and calcium nitrite-based corrosion inhibitor (CN). OPC paste and mortar with TWW were first prepared and compared with the permissible limits specified in ASTM C1602/C1602M – 18 provisions. After that, ten concrete mixes were prepared with different ratios of TWW (0%, 25%, 50%, and 100%), FA (0%, 20%, and 35%), and CN (0% and 3%) and tested for fresh slump and density, compressive and flexural strengths, electrical resistivity, porosity, and chloride permeability. All concrete specimens were cured with fresh water. Concrete hardened properties were tested at 7, 28, and 90 days. Test results revealed that TWW slightly decreased concrete compressive and flexural strengths by 5%–12%, whereas it dramatically increased the porosity and chloride permeability by about 40%. It was also shown that the addition of FA significantly decreased the chloride permeability of TWW concrete by 55%–71%. The optimum FA replacement ratio was observed at 20 wt%. The addition of CN was shown to deteriorate the strength and durability properties of freshwater concrete by 10%–39%. However, combining TWW and CN has improved concrete resistivity, porosity, chloride permeability by 32%, 28%, and 32%, respectively. The optimum concrete properties were obtained using 20 wt% FA and 0% CN. The obtained results were analytically supported by scanning electron microscopy (SEM), energy-dispersive X-ray microanalysis (EDX), and X-ray diffraction (XRD) tests. Moreover, Pearson correlation and linear regressions were performed on the experimental data.

1. Introduction

Global demands for concrete have significantly raised in the past few decades because of the unprecedented growth in the world's population and urbanization [1]. Globally, concrete production exceeds 9 billion tons a year and is expected to increase to 18 billion tons by 2050 [1], causing substantial exploitation of concrete natural resources. Knowing that (i) concrete production consumes about 2 billion tons per year of fresh water globally [2,3]; (ii) fresh water comprises only 2.5% of the Earth's water, of which 0.3% is accessible [4]; (iii) 40% of the world's population might suffer recurring water shortages by 2025 [5]; and (iv) desalination has negative economic and environmental impacts [6–8], it is imperative to investigate the feasibility of utilizing treated domestic wastewater (TWW) in concrete applications. From a sustainability perspective, employing TWW in concrete applications would not only reduce freshwater consumption but also reduce wastewater disposal

costs and environmental impacts [9–12].

There has always been a common perception that TWW is improper for concrete applications. Nevertheless, the use of TWW in place of fresh water has been established in several design codes and standards [13–15]. Furthermore, several researchers have reported on the viability of using secondary and tertiary TWW for concrete applications. Tay and Yip [16] and Ahmed et al. [17] found that the use of reclaimed TWW increased the 28-day mortar compressive strength by 3%–17% compared to freshwater mortar. LEE et al. [18] reported that TWW concrete had 12% and 8% higher compressive strength at 28 and 90 days than freshwater concrete, respectively. Moreover, Cebeci and Saatci [19], Ng et al. [20], Shaikh and Inamdar [21], and Ghrair and Mashaqbeh [22] showed that TWW had no harmful impact on concrete slump, air content, specific gravity, and compressive strength. As well, Arooj et al. [10] and Ahmed et al. [17] showed that the flexural and split tensile strengths of TWW concrete were comparable to those made with

* Corresponding author.

E-mail addresses: aa1104287@qu.edu.qa (A. Abushanab), wael.alnahhal@qu.edu.qa (W. Alnahhal).

<https://doi.org/10.1016/j.job.2021.103240>

Received 1 July 2021; Received in revised form 12 August 2021; Accepted 1 September 2021

Available online 2 September 2021

2352-7102/© 2021 The Authors. Published by Elsevier Ltd. This is an open access article under the CC BY license (<http://creativecommons.org/licenses/by/4.0/>).

Table 1
Chemical compositions of OPC and FA compared to available standards.

Chemical composition (% wt. ¹)	OPC	ASTM C150/C150 M – 20 [59]	FA	ASTM C618 – 19 [63]
Na ₂ O	–	–	0.06	–
SiO ₂	15.84	Minimum 20	55.97	Minimum 50 ²
Fe ₂ O ₃	4.8	Maximum 6	6.63	–
Al ₂ O ₃	3.48	Maximum 6	28.49	–
MgO	2.5	Maximum 5	1.57	–
SO ₃	2.8	Maximum 3	0.51	Maximum 5
P ₂ O ₅	–	–	0.62	–
Cr ₂ O ₃	0.05	–	0.04	–
CL	0.05	–	0.12	–
K ₂ O	0.47	–	1	–
CaO	68.91	–	2.74	Maximum 18
MnO	0.09	–	0.09	–
V ₂ O ₅	0.05	–	0.04	–
Y ₂ O ₃	–	–	0	–
TiO ₂	0.28	–	1.95	–
ZrO ₂	–	–	0.07	–
NiO	–	–	0.02	–
SrO	0.05	–	0.06	–

Note: 1- wt. = weight. 2- For SiO₂, Fe₂O₃, and Al₂O₃.

Table 2
The main properties of the coarse aggregates and sand used.

Property	Sand	Coarse aggregates
Water absorption (%)	0.60	0.72
Bulk density (kg/m ³)	2890	2650
Clay lumps and friable particles (%)	0.10	0.10
Flakiness index (%)	–	6.9
10% fines value (kN)	–	360
Los Angeles abrasion test (%)	–	9
Particle shape index (%)	–	8.2
Material finer than 63 μm (%)	1.1	0.8
Clay lumps and friable particles (%)	0.10	0.10
Acid-soluble chloride (% by weight)	0.02	0.02
Acid-soluble sulfate (% by weight)	0.3	0.1

fresh water. Al-Ghusain and Terro [23], Shekarchi et al. [24], and Noruzman et al. [25] revealed that the setting time of cement paste with TWW was within the allowable limits established in ASTM C94/C94M – 20 provisions [26]. Conversely, Meena and Luhar [11] showed that using secondary and tertiary TWW in concrete decreased concrete slump by 50% and 25%, respectively. Arooj et al. [10] found that the 28-day compressive strength of TWW concrete was 15% lower than that of freshwater concrete. Rao et al. [27] carried out a rapid chloride penetration test (RCPT) and reported that TWW concrete specimens had 30%–36% higher chloride permeability than freshwater concrete specimens. Similar results were also reported by Asadollahfardi et al. [9], Meena and Luhar [11], Saxena and Tembhurkar [28], and Peighambarzadeh et al. [29]. Furthermore, Hassani et al. [30] showed that the chloride ion penetration for freshwater concrete specimens was zero at a depth of 30–35 mm, whereas it was equal to zero at a depth of 35–40 mm for TWW specimens. Asadollahfardi et al. [9] and Magro et al. [31] reported that TWW concrete had more pores and cracks than freshwater concrete.

As presented above, TWW concrete has inferior durability properties in comparison with freshwater concrete due to its high chloride ions and salty suspended particles, which lead to steel corrosion [9]. Numerous studies have reported on the effectiveness of using supplementary cementitious materials (SCM), such as fly ash (FA) [32–38], ground granulated blast furnace slag [39–41], and metakaolin [42,43] in enhancing the chloride binding capacity of concrete and demobilizing chloride ions. SCM absorb the free chloride ions by the calcium-silicate hydrates (C–S–H) gel [44] and Friedel's salt (C₃A·CaCl₂·10H₂O) [36, 45–47]. The latter is a product of the reaction between chloride ions and tricalcium aluminate (C₃A) [48]. Remarkably, FA outperforms other

SCM due to its rapidity in forming Friedel's salt [36]. FA also densifies concrete microstructure through the pozzolanic reactions with calcium hydroxide (Ca(OH)₂) and the formation of the C–S–H gel, and hence decreases the permeability and chloride diffusivity [47,49]. McCarthy and Dhir [50] showed that replacing 40% of ordinary Portland cement (OPC) with FA significantly enhanced the resistance to chloride diffusivity, permeability, and absorption. Sabet et al. [51] found that 10% and 20% FA decreased the chloride diffusion coefficient by 40.5% and 59.5%, and enhanced the electrical resistivity by 257% and 495%, respectively, compared to 100% OPC concrete. Similar results were also obtained by Wang et al. [52].

Likewise, calcium nitrite-based corrosion inhibitor (CN) has been widely used in concrete exposed to marine environments due to its outperformance in strengthening the steel passivation layer [53–55]. Lopez-Calvo et al. [53] reported that the combination of CN and FA showed an enhancement in the compressive strength at later ages. Milla et al. [56] revealed that CN concrete showed satisfactory self-healing results. However, the mechanical properties of CN concrete were significantly lower than that of conventional concrete. Berke and Hicks [57] showed that CN concrete had a lower steel corrosion rate than conventional concrete without CN. Sideris and Savva [58] showed that concrete carbonation depth was decreased with the addition of CN.

Even though several studies were carried out on the properties of TWW concrete, discrepancy results were reported among the previous studies, as the characteristics of TWW are influenced to a large degree by TWW origin and level of cleanliness. There are also no studies on the influence of TWW, produced in the State of Qatar, on the mechanical and durability properties of concrete. Moreover, previous studies investigated separately the effect of TWW, FA, and CN on concrete properties. However, there is a lack of the combined effect of TWW, FA, and CN on the mechanical and durability properties of concrete. Hence, the objective of the present study was to evaluate concrete slump, compressive and flexural strengths, electrical resistivity, porosity, and chloride permeability of concrete incorporating TWW, FA, and CN simultaneously. Furthermore, the experimental results were analytically supported by scanning electron microscopy (SEM), energy-dispersive X-ray microanalysis (EDX), and X-ray diffraction (XRD) tests.

2. Materials and methods

A total of 190 concrete specimens, including 130 cylinders and 60 prisms, were prepared and tested. All specimens were kept in a fresh-water curing tank until the testing date. The details of the material used, concrete mix proportions, casting process, and testing methods are presented in the following subsections:

2.1. Materials

2.1.1. OPC, FA, CN, and aggregates

A commercial OPC type CEM I 42.5R, complying with ASTM C150/C150M – 20 standards [59], with a particle size range from 10 to 90 μm was used in this study. Class F FA with a particle size range from 3 to 55 μm was used at replacement ratios of 20% and 35% by weight of cement. The specific gravity of OPC and FA was 3.15 and 2.23, respectively (ASTM C188 – 17 [60]). The moisture content of FA was 0.5% (ASTM C311/C311 M – 18 [61]). The main chemical characteristics of both OPC and FA were determined using X-ray fluorescence (XRF) analysis [62] and compared with ASTM C150/C150 M – 20 [59] and ASTM C618 – 19 [63] limitations, as shown in Table 1. It should be noted that the total percentage of oxides in Table 1 is not 100% because lighter oxides are not detected by the equipment. It could be seen that FA had a higher amount of silica compared to OPC. In addition, a 3% CN admixture with a minimum of 30% calcium nitrite and specific gravity of 1.3 was employed as a corrosion inhibitor. Concrete constituents also include wash sand and 19-mm maximum size coarse gabbro aggregates (GA). The physical characteristics of both wash sand and coarse

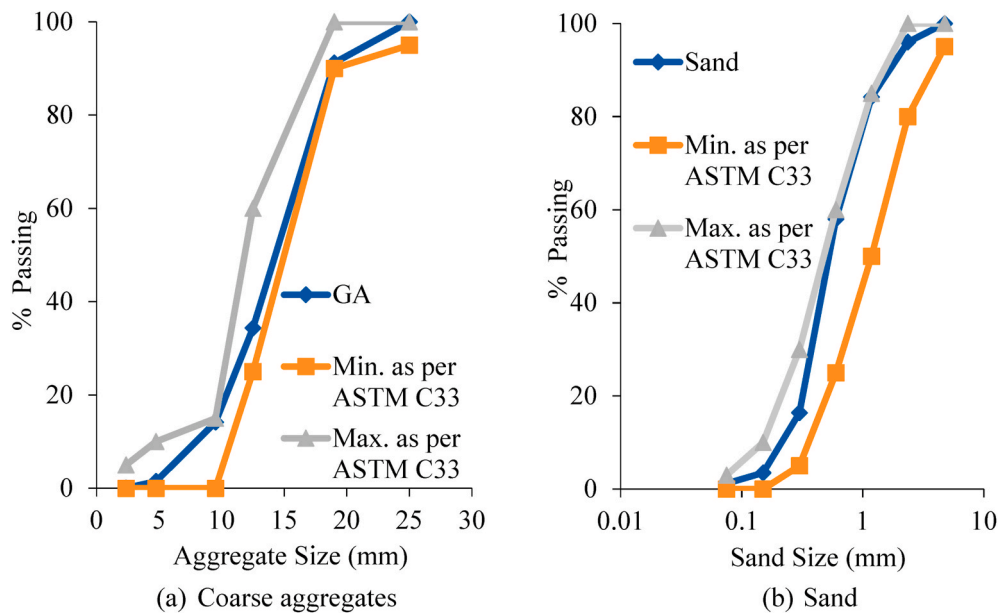


Fig. 1. Gradation of coarse aggregates and sand.

aggregates are shown in Table 2. The gradation of coarse aggregates and sand with respect to ASTM C33/C33M – 18 limits [64] are plotted in Fig. 1(a) and (b).

2.1.2. Water

Two types of mixing water were used in this study: fresh water and domestic tertiary TWW, designated herein as TWW. The freshwater used was satisfying the World Health Organization standards [65], and the TWW was collected from a local wastewater treatment plant in Qatar. Chemical characterization of both water types was performed as per the standard methods for examining water and wastewater [66] and reported in Table 3. As shown in the table, the characteristics of both water were within the acceptable limits for reinforced concrete elements specified by ASTM C1602/C1602M – 18 [13], BS EN 1008:2002 [15], and Qatar Construction Specifications (QCS)-2014 [67] standards. Furthermore, the TWW had comparable pH, total suspended solids (TSS), residual chlorine, dissolved oxygen, biochemical oxygen demand, and chemical oxygen demand with fresh water. However, total dissolved solids (TDS), chloride, sulfate, iron, zinc, and phosphate in the TWW were higher than those in fresh water. As shown in Table 3, TWW used by Asadollahfardi et al. [9], Arooj et al. [10] and Ahmed et al. [17] also met the requirements of QCS 2014 [67], ASTM C1602/C1602M – 18 [13], and BS EN 1008:2002 [15] standards. Nonetheless, the TWW characteristics of these studies were not the same as those of our study. TSS concentration in this research was 8 to 10 times lower than that in Asadollahfardi et al. [9], Arooj et al. [10], and Ahmed et al. [17]. Whereas TDS concentration in the utilized TWW was equivalent to that in Arooj et al. [10], it was 52% and 152% higher than that in Asadollahfardi et al. [9] and Ahmed et al. [17], respectively. It could also be observed that the TWW used in this study had significantly higher chloride and sulfate concentration than the TWW used in the previous studies.

2.2. Concrete mix proportions

A total of 10 concrete mixes were prepared in this study with various TWW, FA, and CN replacement ratios. Concrete mix proportions are shown in Table 4. The designation of concrete mixes is summarized in Fig. 2. Mix T0-F0-C0 was designed in accordance with ASTM C192/C192M – 19 [68] standards and considered as the reference mix. Multiple trials for mix T0-F0-C0 were performed to achieve a 28-day

compressive strength of 50 MPa. Other mixes were prepared by (i) replacing 25%, 50%, and 100% of fresh water weight with TWW; (ii) replacing 20% and 35% of OPC weight with FA; and (iii) adding 3% CN by OPC weight. All concrete mixes maintained a constant water-to-binder ratio (W/B) and superplasticizer of 0.45 and 0.2%, respectively, to evaluate the impact of the aforementioned ingredients on concrete fresh slump.

2.3. Test methods

2.3.1. Characterization of cement paste and mortars

According to ASTM C1602/C1602M – 18 provisions [13], before using non-potable water in concrete, OPC setting time and mortar compressive strength at 7 days shall be tested and compared with their counterparts with fresh water. The initial and final setting time of OPC paste was measured as per ASTM C191-19 provisions [69]. The mortar compressive strength was determined as per ASTM C109/C109M-20b provisions [70]. According to ASTM C1602/C1602M – 18 [13], OPC setting time shall not be 1 h earlier or 1.5 h later than the setting time of reference OPC paste, and the 7-day mortar compressive strength shall not be less than 90% of the average compressive strength of the fresh-water mortar.

2.3.2. Fresh and mechanical properties of concrete

The slump flow and density of fresh concrete were immediately determined after casting as per ASTM C143/C143M-15a [71] and ASTM C138/C138M-17a [72] provisions, respectively. In addition, concrete compressive strength tests were conducted on 100 × 200 mm cylindrical specimens according to ASTM C39/C39M – 20 provisions [73]. Three cylinders were prepared and tested for each mix after 7, 28, and 90 days of curing at a loading rate of 0.2 MPa/s. Furthermore, the flexural strength of concrete was determined on beam-type prisms with dimensions of 100 × 100 × 500 mm as per ASTM C78/C78M – 18 provisions [74]. Three prisms for each concrete mix were tested after 28 and 90 days of curing with a loading rate of 0.58 kN/s.

2.3.3. Durability characteristics of concrete

2.3.3.1. *Electrical resistivity.* Concrete electrical resistivity was evaluated using a four-point Wenner probe Giatec® resistivity meter (Fig. 3 (a)) as per AASHTO TP 95 standards [75]. For each mix, three

Table 3
Chemical compositions of fresh water and TWW compared to available standards and previous studies.

Component	Unit	Fresh water	TWW utilized in this study	TWW utilized in Asadollahfardi et al. [9]	TWW utilized in Arooj et al. [10]	TWW utilized in Ahmed et al. [17]	QCS 2014 [67]	ASTM C1602/C1602M – 18 [13]	BS EN 1008:2002 [15]
pH	-	8.1	7.8	7.7	7.2	7.9	6.5–9.0	-	>4
TDS	mg/l	93	1690	170	1110	670	2000	50000	2000
TSS	mg/l	2	3	30	21	14	-	-	100
Chloride (Cl ⁻)	mg/l	14.1	511	55	175	-	-	500 for PRC	500 for PRC
Residual chlorine (Cl ₂)	mg/l	<0.1	<0.1	-	-	-	-	1000 for RC	1000 for RC
Dissolved oxygen	mg/l	9.4	8	-	-	-	-	-	4500 for PC
Sulfate (SO ₄ ²⁻)	mg/l	6	490	180	170.7	100	2000	3000	2000
Iron (Fe ⁺²)	mg/l	0.0135	0.077	-	-	-	-	-	-
Zinc (Zn ⁺²)	mg/l	0.0046	0.1051	-	-	-	100	-	-
Phosphate (PO ₄)	mg/l	<0.03	9.19	-	-	-	-	-	-
BOD ₅	mg/l	<5	5	30	43.5	7	-	-	-
COD	mg/l	<10	<10	92	72	<10	50	-	-

Note: 1- TDS = total dissolved solids, TSS = total suspended solids, BOD₅ = biochemical oxygen demand, COD = chemical oxygen demand, QCS = Qatar construction specification, PRC = prestress concrete, RC = reinforced concrete, and PC = plain concrete.

cylindrical specimens with dimensions of 100 × 200 mm were tested at 7, 28, and 90 days of curing. Table 5 presents the corrosion risks as a function of the resistivity values. Higher resistivity indicates less corrosion risk and vice versa.

2.3.3.2. *Porosity*. Concrete porosity (i.e., void content) tests were performed based on procedures established in ASTM C1754/C1754M – 12 provisions [76]. Two cylinders with dimensions of 100 × 200 mm for each concrete mix were prepared and cured for 28 and 90 days. The specimens were then sliced into four cylinders of 50 mm height. After that, the sliced specimens were dried in an oven at 38 °C for 24 h, and the dry weight was recorded. The specimens were reweighed until a difference of 0.5% between two consecutive weights was achieved. Subsequently, the specimens were fully immersed in water for 30 min and weighed. The porosity (void content) was finally calculated according to Eq. (1).

$$Void\ content = \left[1 - \left(\frac{K \times (A - B)}{\rho_w \times D^2 \times L} \right) \right] \times 100 \tag{1}$$

where *K* is a constant (1273240 mm³kg/m³g), *A* is the dry weight (g), *B* is the submerged weight (g), *ρ_w* is the water density (kg/m³), *D* is the specimen’s diameter, and *L* is the specimen’s height.

2.3.3.3. *Rapid chloride penetration test (RCPT)*. RCPT indicates how easily chloride ions can penetrate concrete. The test was performed as per ASTM C1202-19 standards [77] on two 100 × 50 mm cylinders sliced from the middle of 200-mm height cylinders at 28 and 90 days (Fig. 3(b)). The specimens were first conditioned in an oven at 50 °C for three days. Next, silicon epoxy was applied to the specimens’ circumferences. Then, the specimens were vacuumed in a desiccator for 3 h under 50 mmHg, followed by a fully immersing in deaerated water for 18 h. After that, the conditioned specimens were placed inside two molds, of which one was filled with a 3% concentrated sodium chloride (NaCl) solution and the other one with 0.3 N concentrated sodium hydroxide (NaOH) solution. Finally, a potential difference of 60 V was applied on the test molds for 6 h, and the current flows were reported at a 30-min interval. The total charges transferred (*Q*) were calculated according to Eq. (2).

$$Q = 900(I_0 + 2I_{30} + 2I_{60} + \dots + 2I_{300} + 2I_{330} + I_{360}) \tag{2}$$

where *I*₀, *I*₃₀, *I*₆₀, etc. are the applied current (Amperes) at the beginning, after 30 min, after 60 min, etc.

2.3.4. *Microstructural analysis*

Microstructural analysis was performed on fractured sections using a NOVA NANOSEM 450 scanning electron microscope as per ASTM C1723-16 provisions [78]. The analysis performed included (a) SEM to study the morphology of concrete and (b) EDX to determine the chemical composition of concrete. Furthermore, XRD analysis was performed using a PAN analytical® EMPYREAN to study the mineralogy of the cementitious products.

3. Results and discussion

3.1. Characteristics of OPC paste and mortar

The initial and final setting time of OPC paste made with fresh water and TWW is shown in Table 6. The results showed that replacing fresh water with TWW increased both the initial and final setting time of OPC paste by 20.7% and 29.2%, respectively, owing to the presence of zinc and phosphate salts in TWW, which delayed the hydration of C₃A [18]. Despite that increase, the results are within the permissible limits specified in ASTM C1602/C1602M – 18 standards [13]. It is worth mentioning that the increase in the setting time of TWW paste is relatively lower than other studies conducted by Asadollahfardi et al. [9],

Table 4
Concrete mix proportions.

Mix	Ingredients (kg/m ³)							
	Fresh water	TWW	OPC	Coarse aggregates	Sand	FA	CN	SP
T0-F0-C0	156.4	0	349.2	1075.5	708.1	0	0	0.7
T25-F0-C0	117.3	39.1	349.2	1075.5	708.1	0	0	0.7
T50-F0-C0	78.2	78.2	349.2	1075.5	708.1	0	0	0.7
T100-F0-C0	0	156.4	349.2	1075.5	708.1	0	0	0.7
T0-F20-C0	156.4	0	279.3	1075.5	708.1	69.8	0	0.7
T100-F20-C0	0.0	156.4	279.3	1075.5	708.1	69.8	0	0.7
T100-F35-C0	0	156.4	227.0	1075.5	708.1	122.2	0	0.7
T0-F0-C3	156.4	0	349.2	1075.5	708.1	0	10.5	0.7
T100-F0-C3	0	156.4	349.2	1075.5	708.1	0	10.5	0.7
T100-F20-C3	0	156.4	279.3	1075.5	708.1	69.8	10.5	0.7

Note: SP = superplasticizer.

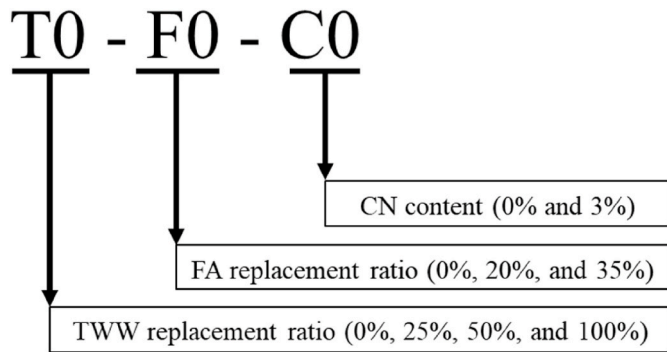


Fig. 2. Designation of concrete mixes.

Table 6
Setting time of cement paste.

Mixing water	Setting time (minutes)	
	Initial	Final
Fresh water	198	205
TWW	239	265

Table 7
Compressive strength of cement mortars at 7 days.

Type	Mixing water	Curing water	Compressive strength (MPa)
1	Fresh water	Fresh water	34.96
2	TWW	Fresh water	37.12
3	TWW	TWW	35.81



(a)



(b)

Fig. 3. Durability test setups: (a) electrical resistivity and (b) RCPT.

Table 5
Corrosion risks as a function of concrete resistivity values [75].

Resistivity (kΩ•cm)	Corrosion Risk
<12	High
12–21	Moderate
21–37	Low
37–254	Very low
>254	Negligible

Table 8
Concrete fresh properties.

Mix	Slump (mm)	Density (kg/m ³)
T0-F0-C0	86	2473
T25-F0-C0	83	2467
T50-F0-C0	85	2486
T100-F0-C0	91	2448
T0-F20-C0	135	2465
T100-F20-C0	145	2506
T100-F35-C0	185	2501
T0-F0-C3	180	2507
T100-F0-C3	190	2521
T100-F20-C3	210	2535

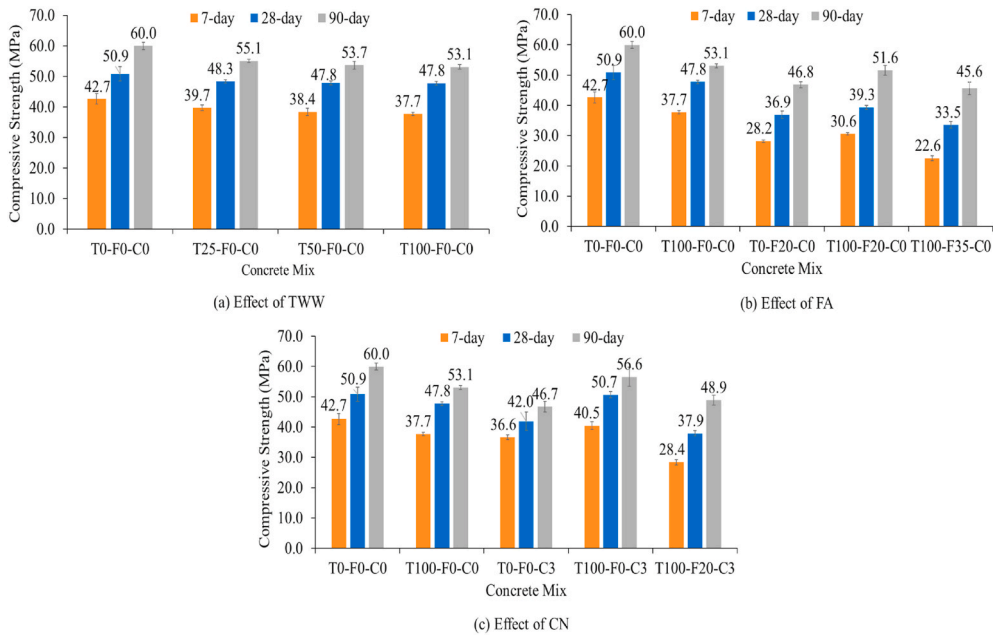


Fig. 4. Concrete compressive strength at different curing ages.

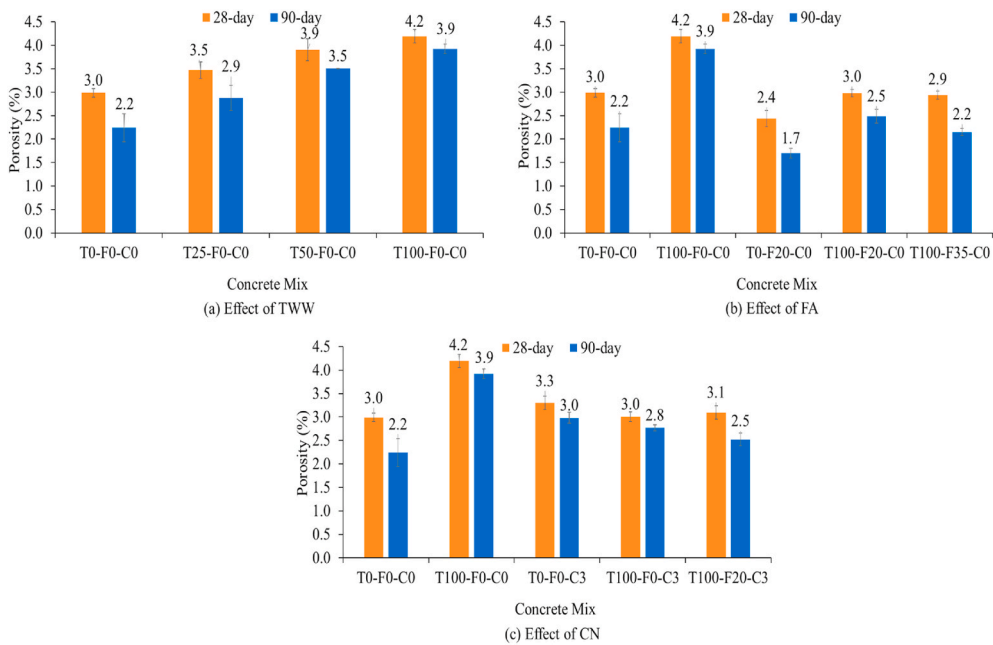


Fig. 5. Flexural tensile strength results at different curing ages.

Saxena and Tembhurkar [28], and Magro et al. [31]. The results also indicated that mixing and curing OPC mortars by TWW slightly increased the 7-day compressive strength by 2%–6% (Table 7), which can be considered a normal discrepancy in the experimental results. The compressive strength results align with the allowable limits of ASTM C1602/C1602M – 18 standards [13].

3.2. Fresh and mechanical properties of concrete

3.2.1. Slump and density of fresh concrete

Fresh concrete slump and density results are listed in Table 8. The results indicated that TWW did not affect concrete workability, as the slump of mixes T25-F0-C0, T50-F0-C0, and T100-F0-C0 varied by 3.4%, 1.2%, and 5.5%, from mix T0-F0-C0, respectively. This is attributed to

the low suspended solids in the TWW used, which did not affect the TWW weight and concrete flow. Also, Neville [79] reported that concrete flow depends mainly on the water quantity, not quality. The obtained results were in agreement with Al-Ghusain and Terro [23], Shekarchi et al. [24], and Noruzman et al. [25]. The presented results also showed that replacing 20 wt% and 35 wt% OPC by FA in mixes T0-F20-C0, T100-F20-C0, and T100-F235-C0 increased concrete slump by 56%–115%. Both types of water showed a similar improvement with FA. This is due to the small spherical shape of FA, which resulted in less frictional losses with other ingredients. As well, decreasing OPC weight resulted in an excess amount of water and thus increased concrete slump. These results are consistent with Berndt [80]. Likewise, adding 3% CN in mixes T0-F0-C3, T100-F0-C3, and T100-F20-C3 increased concrete slump by 109.3%, 120.9%, and 144.2%, respectively in

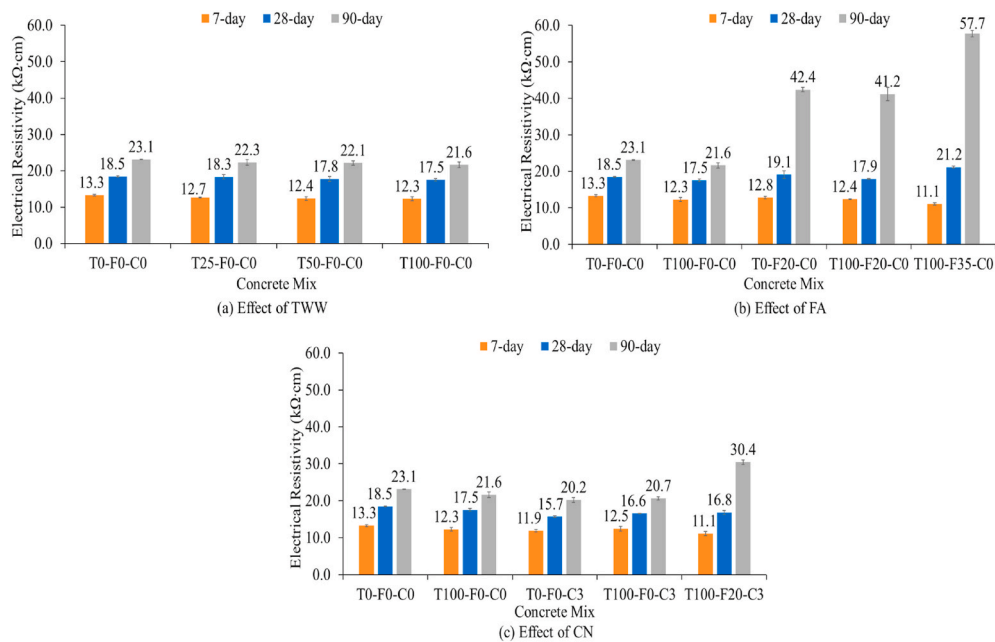


Fig. 6. Electrical resistivity at different curing ages.

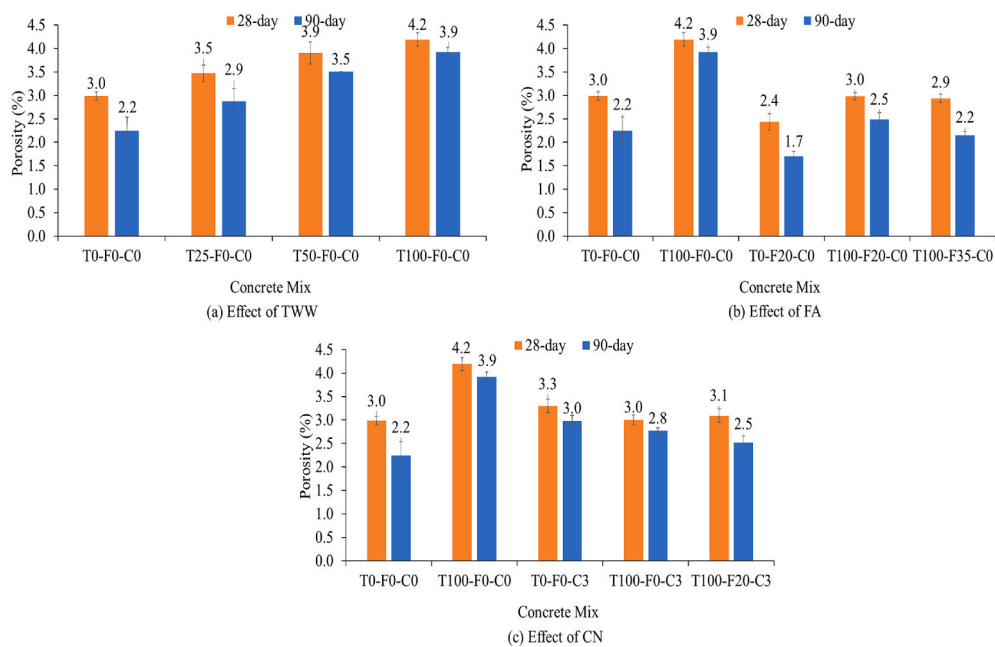


Fig. 7. Concrete porosity at different curing ages.

comparison with the reference mix. That was because the CN used was in a liquid state, which consequently decreased viscosity and increased the liquidity of concrete [81]. A similar observation was found by Lopez-Calvo et al. [53] and Li et al. [82], who reported a 13%–76% increase in the concrete slump with CN. Furthermore, incorporating both FA and CN in mix T100-F20-C3 has further enhanced concrete flow by 44.8% and 10.5% compared to mixes T100-F20-C0 and T100-F0-C3, respectively.

It could also be observed from Table 8 that TWW had no effect on concrete fresh density. That was because fresh water and TWW have approximately a similar density. The results of Al-Ghusain and Terro [23] and Saxena and Tembhurkar [28] also confirmed that TWW has little-to-no effect on concrete density. Similarly, incorporating FA and

CN in concrete showed no harmful effect on concrete fresh density, owing to their low proportions in the mixes [82].

3.2.2. Compressive strength

The compressive strength test results at 7, 28, and 90 days are presented in Fig. 4. It was observed that all mixes exhibited higher compressive strength at higher curing periods, owing to the cement hydration progress over time, which produced more cementitious products and thus decreased concrete pores and enhanced the bond strength between cement and aggregates [9]. It could also be seen that the substitution of 25 wt%, 50 wt%, and 100 wt% of fresh water by TWW decreased the compressive strength by 5%–12% at all ages (Fig. 4(a)). This is mainly attributed to the dissolved oxygen and suspended solids in

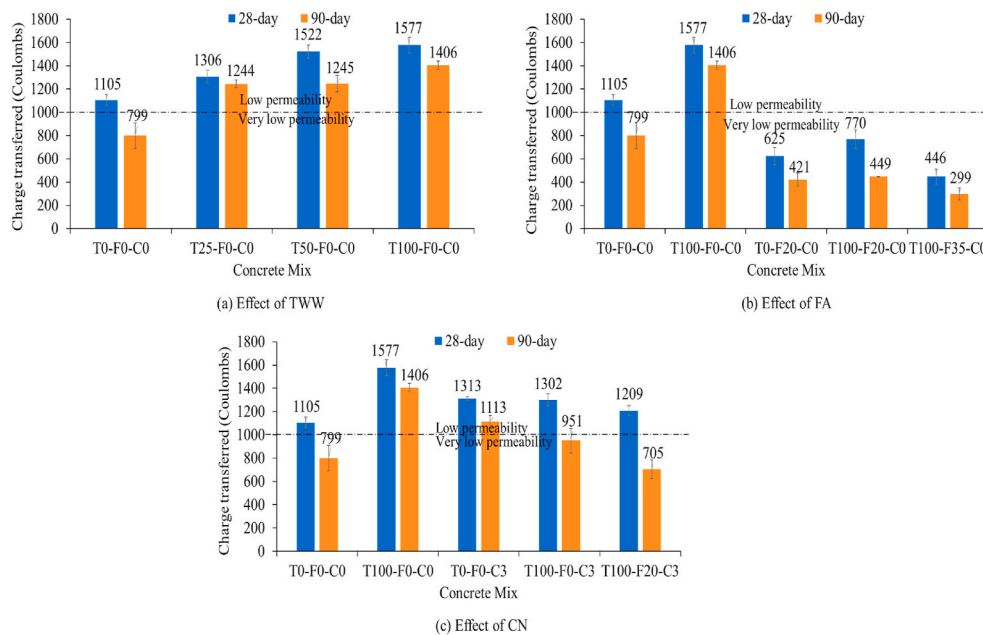


Fig. 8. RCPT results at different curing ages.

TWW, which affected concrete permeability. The decrease in the compressive strength with TWW might also be attributed to the presence of zinc and phosphate salts in TWW, which delayed the hydration of C_3A [18]. Moreover, the rate of increase in the compressive strength with time decreased as the TWW replacement ratio increased. For instance, compared to the 28-day compressive strength results, specimen T0-F0-C0 improved by 17.88%, while specimen T100-F0-C0 improved by 11.1% at 90 days. This is ascribed to the reaction of sulfate ions in TWW with $Ca(OH)_2$ and C_3A , which, in turn, formed additional ettringite and disintegrated concrete matrix [83]. The obtained results agree with Asadollahfardi et al. [9], who reported a 6% decrease in the compressive strength of TWW concrete specimens.

Incorporating 20 wt% FA in mixes T0-F20-C0 and T100-F20-C0 decreased the 7 and 28-day compressive strength by an average of 30.7% and 25.6%, respectively, compared to the reference mix (Fig. 4 (b)). Increasing FA replacement ratio to 35% in mix T100-F35-C0 further decreased the compressive strength by 40.6%. This reduction has occurred due to the decreased cement content, which decreased the hydration products and the bond strength between cement and aggregates. Nevertheless, due to the pozzolanic reactions with $Ca(OH)_2$ and its consequences in densifying concrete microstructure, the reduction rate at 90 days was decreased to 22%, 14%, and 24% for mixes T0-F20-C0, T100-F20-C0, and T100-F35-C0, respectively. The increase in the compressive strength of mix T100-F20-C0 compared to T0-F20-C0 indicates that FA filled concrete cracks and voids induced by TWW and resulted in a more densified microstructure. Additionally, the gain in strength of TWW specimens with FA was considerably higher than those made without FA due to the pozzolanic reaction, which consumed $Ca(OH)_2$ and prevented its reaction with sulfate ions.

Fig. 4(c) shows that adding 3% CN in mix T0-F0-C3 decreased the compressive strength by 14.3%, 17.5%, and 22.2% at 7, 28, and 90 days, respectively, compared to its respective without CN. This is primary attributed to the accelerated formation of ettringite (i.e., $C_6AS_3H_{32}$) in the presence of calcium, which significantly increased concrete micropores [54]. By contrast, mix T100-F0-C3 had 7.4%, 6.1%, and 6.6% higher compressive strength at 7, 28, 90 days, respectively, than mix T100-F0-C0. This could be explained by the presence of sulfate in TWW, which reacted with ettringite and C_3A , and produced calcium monosulphoaluminate hydrate (i.e., C_4ASH_{12}) [84]. A combination of 20 wt% FA and 3 wt% CN in mix T100-F20-C3 showed comparable results to

T100-F20-C0 at all curing periods. Similarly, Lopez-Calvo et al. [53] achieved higher compressive strength for freshwater concrete made with CN and exposed to a marine environment.

3.2.3. Flexural tensile strength

The variations in the flexural tensile strength results with different substitutions of TWW, FA, and CN are shown in Fig. 5. It could be noticed that the 90-day prisms had 18%–55% higher flexural tensile strength than the 28-day prisms, owing to the cement hydration progress with time, which enhanced the interfacial transition zone (ITZ) layer between the cement matrix and aggregates. It could also be observed that concrete flexural strength gradually decreased by increasing the TWW replacement ratio. Mixes T25-F0-C0, T50-F0-C0, and T100-F0-C0 showed 1%, 5.5%, and 7.9% lower flexural strength at 28 days and 6.1%, 7.6%, and 10.6% at 90 days than mix T0-F0-C, respectively, as shown in Fig. 5(a). This is attributed to the suspended solids in TWW, which penetrated and weakened the ITZ layer between the cement matrix and aggregates. Asadollahfardi et al. [9] also reported a slight decrease in the flexural strength with TWW. Similar to compressive strength results, the rate of increase in the flexural strength with time decreased as the TWW replacement ratio increased, owing to the reaction of sulfate ions in TWW with $Ca(OH)_2$ and C_3A , which disintegrated concrete matrix [83].

Incorporating FA in mixes T0-F20-C0, T100-F20-C0, and T100-F35-C0 decreased the 28-day flexural strength by 11.3%, 12.2%, and 24.5%, respectively, compared to their counterparts without FA (Fig. 5(b)). This is due to the decreased adhesive force between aggregates and cement, resulting from reducing the amount of OPC [85]. However, the 90-day prisms showed comparable results to their counterparts without FA, attributable to the pozzolanic reactions with $Ca(OH)_2$, which densified concrete microstructure [85].

Meanwhile, Fig. 5(c) shows that adding 3% CN decreased the 28 and 90-day flexural strength of mix T0-F0-C3 by 17% and 13% compared to that of the reference mix, respectively. The reduction might have occurred because CN has rapidly accelerated the formation of ettringite needles, which consequently increased concrete voids and cracks and affected the ITZ layer between the cement matrix and aggregates [54]. Conversely, mix T100-F0-C3 reported 7.8% and 16.3% higher flexural strength at 28 days than mixes T0-F0-C0 and T100-F0-C0, respectively. This increase is probably related to the presence of sulfate ions in TWW.

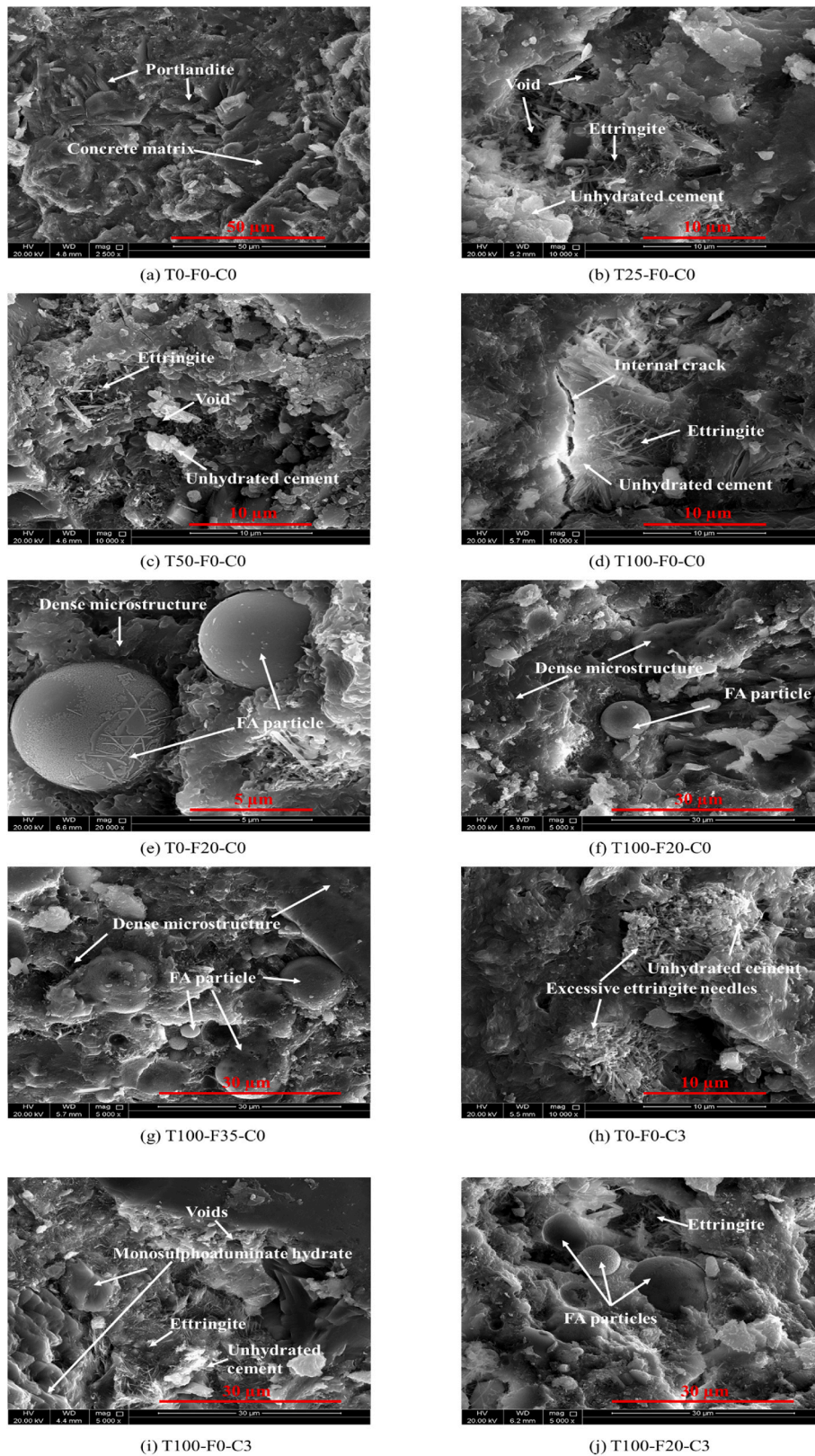
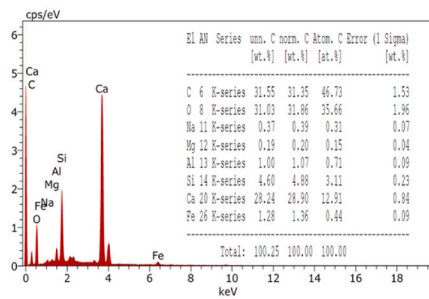


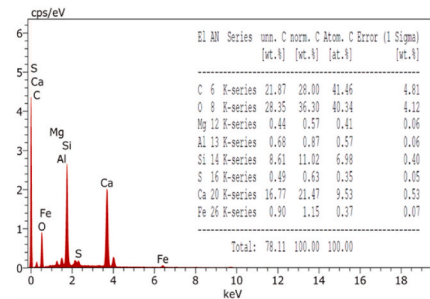
Fig. 9. SEM images for all concrete mixes.

Sulfate ions reacted with ettringite and C_3A and formed calcium monosulphoaluminate hydrate, which decreased the micropore volume and improved the ITZ layer between aggregates and cement [84]. By contrast, combining both FA and CN in mix T100-F20-C3 decreased the 28 and 90-day flexural strength by 31.4% and 16.5%, respectively,

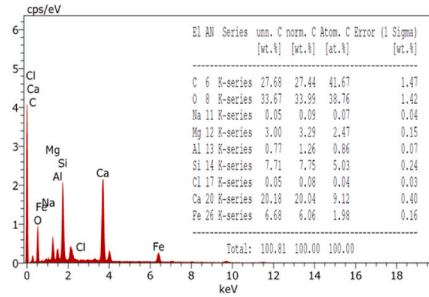
compared to that of T100-F0-C3. This likely happened because FA absorbed sulfate ions and decreased the rate of formation of calcium monosulphoaluminate hydrate [84].



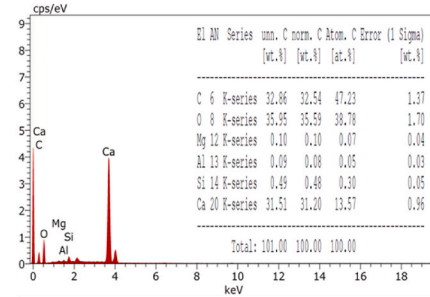
(a) T0-F0-C0



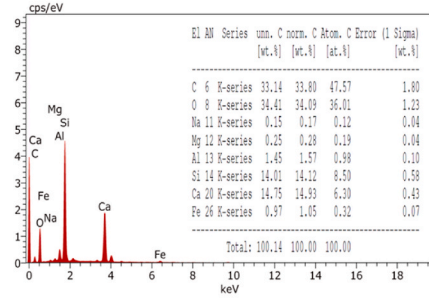
(b) T25-F0-C0



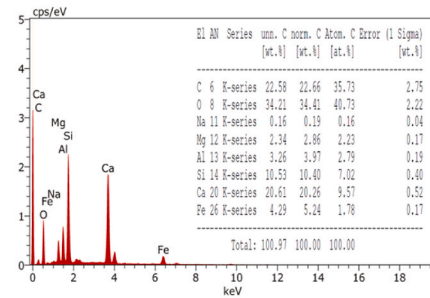
(c) T50-F0-C0



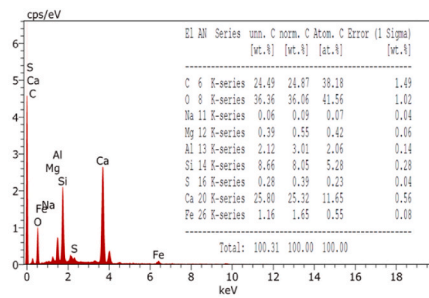
(d) T100-F0-C0



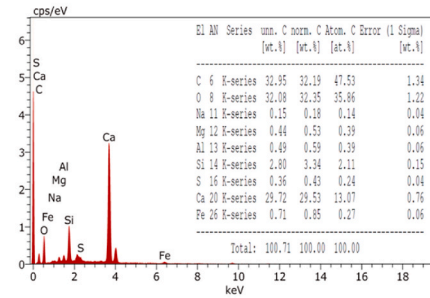
(e) T0-F20-C0



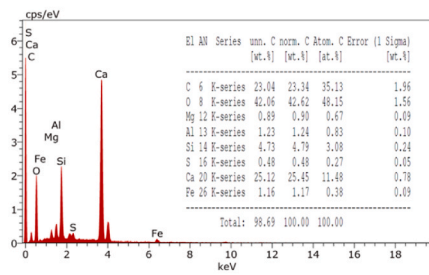
(f) T100-F20-C0



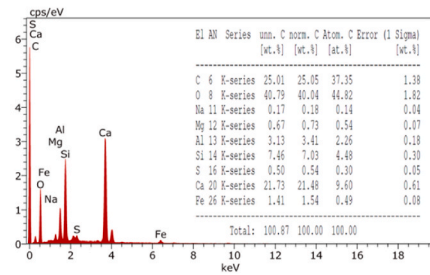
(g) T100-F35-C0



(h) T0-F0-C3



(i) T100-F0-C3



(j) T100-F20-C3

Fig. 10. EDX microanalysis results for all concrete mixes.

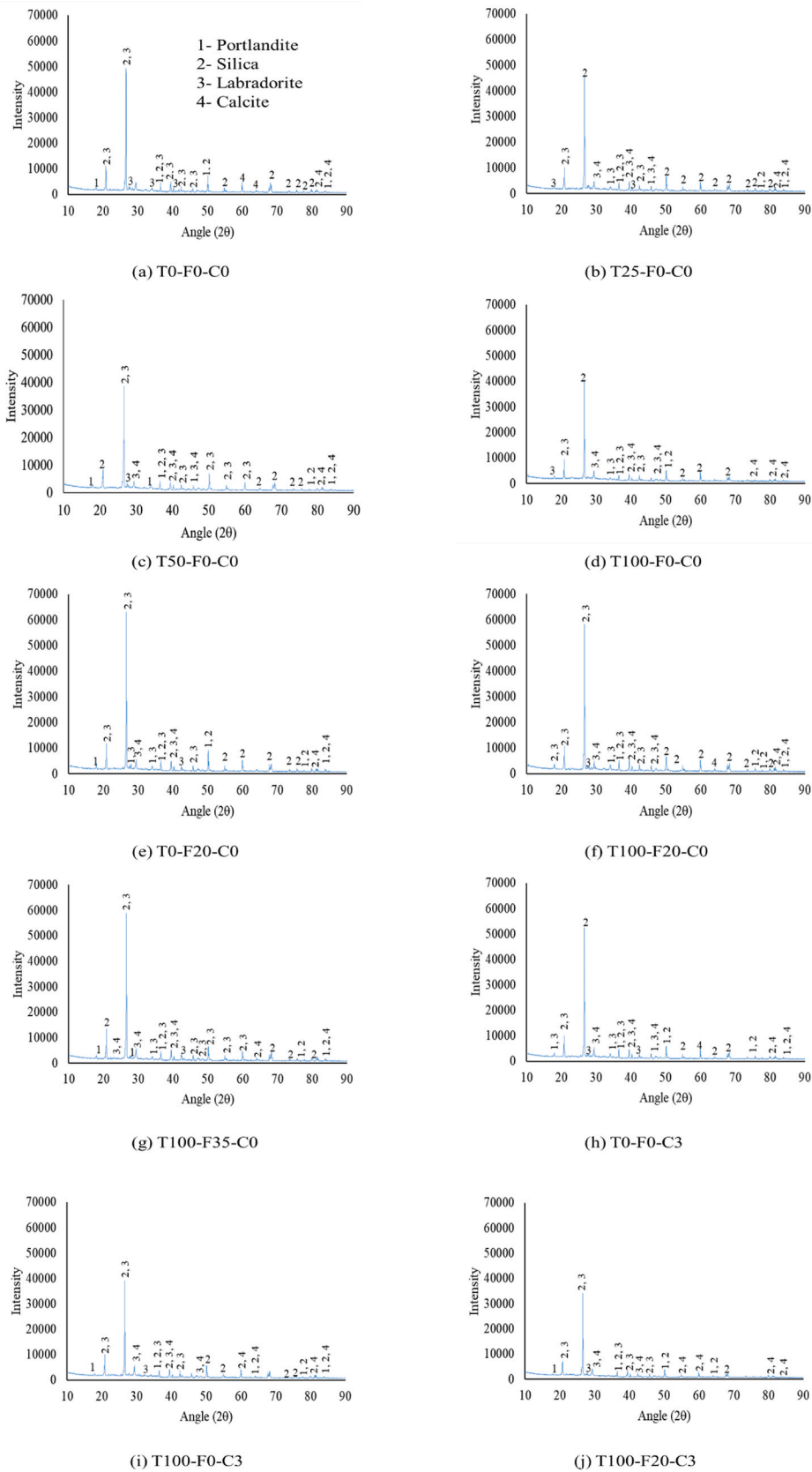


Fig. 11. XRD peaks for all concrete mixes.

Table 9
Correlation coefficient of groups I, II and III.

		Compressive strength	Flexural strength	Electrical resistivity	Porosity
Group I	Flexural strength	0.966	–	–	–
	Electrical resistivity	0.929	0.987	–	–
	Porosity	–0.792	–0.710	–0.593	–
	RCPT	–0.818	–0.726	–0.617	0.951
Group II	Flexural strength	0.925	–	–	–
	Electrical resistivity	0.764	0.796	–	–
	Porosity	–0.594	–0.851	–0.702	–
	RCPT	–0.437	–0.528	–0.828	0.573
Group III	Flexural strength	0.971	–	–	–
	Electrical resistivity	0.353	0.354	–	–
	Porosity	–0.612	–0.596	–0.911	–
	RCPT	–0.452	–0.442	–0.959	0.939

3.3. Durability properties of concrete

3.3.1. Electrical resistivity

Electrical resistivity results for all concrete mixes at 7, 28, and 90 days are presented in Fig. 6. Similar to the results of the compressive and flexural strengths, it was noticed that the electrical resistivity increased as the curing period of concrete increased because of the cement hydration progress with time. As anticipated, TWW slightly decreased concrete electrical resistivity by 1%–6.5% at all curing periods (Fig. 6 (a)). This decrease might be due to the suspended solids in TWW, which increased concrete pores and expedited the movement of electrons. A study performed by Shekarchi et al. [24] showed that concrete resistivity dropped by 16% when fresh water was replaced by TWW for concrete mixing and curing.

Despite the decrease encountered in the compressive and flexural strengths with FA, it could be recognized from Fig. 6(b) that incorporating FA at replacement ratios of 20 wt% and 35 wt% significantly enhanced concrete electrical resistivity at 28 and 90 days. For example, specimens T0-F20-C0, T100-F20-C0, and T100-F35-C0 reported 83.5%, 78.4%, and 149.8% higher electrical resistivity than T0-F0-C0, respectively. Additionally, specimens T0-F20-C0, T100-F20-C0, and T100-F35-C0 had a “very low” corrosion risk, while T0-F0-C0 had a “low” corrosion risk, as per the classifications established in AASHTO TP 95 standards [75] (see Table 5). This is attributed to the pozzolanic reactions with $\text{Ca}(\text{OH})_2$, which produced C–S–H gel and decreased concrete permeability. The obtained results agree well with Kurda et al. [86] for freshwater concrete mixes.

In agreement with the compressive and flexural strength, Fig. 6(c) reveals that incorporating 3% of CN deteriorated the electrical resistivity at all curing ages. For instance, the 28-day electrical resistivity of mixes T0-F0-C3 had 15.13% lower electrical resistivity than T0-F0-C0. That was because CN has excessively formed ettringite needles, which disintegrated concrete matrix and increased concrete pores [84]. However, the rate of reduction in the electrical resistivity of T100-F0-C3 was 32% lower than that of T0-F0-C3, owing to the formation of calcium monosulphoaluminate hydrate in the presence of sulfate ions in TWW [84]. Furthermore, combining FA and CN in mix T100-F20-C3 increased the electrical resistivity by an average of 48.67% compared to T0-F0-C3 and T100-F0-C3.

3.3.2. Porosity

Fig. 7 shows concrete porosity test results at 28 and 90 days. It could be noticed that concrete specimens at 90 days recorded 7%–27% lower porosity than that at 28 days, owing to the cement hydration progress with time and secondary pozzolanic reactions. In conformance with electrical resistivity test results, it was observed that concrete porosity increased with increasing the TWW replacement ratio (Fig. 7(a)). For instance, specimens T25-F0-C0, T50-F0-C0, and T100-F0-C0 had 23%, 30%, and 40% higher porosity at 28 days than T0-F0-C0, respectively.

This is due to the dissolved oxygen and suspended solids in TWW, which slightly altered the cement hydration process and increased concrete pores [25].

Moreover, Fig. 7(b) shows that incorporating 20 wt% FA in specimens T0-F20-C0 and T100-F20-C0 decreased concrete porosity at 28 days by an average of 20.7% and 29.3%, respectively, in comparison with their counterparts with no FA. By increasing the FA replacement ratio to 35% in T100-F35-C0, the porosity further decreased by 31% compared to T100-F0-C0. This is ascribed to the increased particle size distribution and secondary reactions with $\text{Ca}(\text{OH})_2$, which densified concrete microstructure [87].

Conversely, CN showed varying levels of effect with fresh water and TWW. The 28 and 90-day porosity of mix T0-F0-C3 increased by 10% and 27% compared to the reference mix, respectively (Fig. 7(c)). As mentioned previously, this increase is linked to the rapid and excessive formation of ettringite needles, which increased concrete micropores [54]. However, mix T100-F0-C3 reported 21% and 28% lower porosity at 28 and 90 days than T100-F0-C0, respectively. This is attributed to the presence of sulfate in TWW, which reacted with ettringite and C_3A and formed calcium monosulphoaluminate hydrate [84]. Moreover, the combination of CN and FA in T100-F20-C3 further decreased the 90-day porosity by 11% compared to T100-F0-C3 due to the additional effect of FA.

3.3.3. The rapid chloride penetration test

Fig. 8 presents the RCPT results for all concrete mixes. Confirming the electrical resistivity and porosity test results, specimens T25-F0-C0, T50-F0-C0, and T100-F0-C0 recorded 18.2%, 37.7%, and 42.7% higher Coulomb charges at 28 days than specimen T0-F0-C0, respectively, as appeared in Fig. 8(a). This is fundamentally attributed to the high chloride ions in TWW compared to that in fresh water. Despite the increase in the RCPT results with TWW, the four specimens were classified as “low permeability” as per the classifications established in ASTM C1202-19 standards [77], indicating that the four mixes were durable. Furthermore, the specimens reported 5%–28% lower charges at 90 days due to cement hydration progress with time, which produced more cementitious products and consequently decreased concrete pores. The obtained results are in line with Saxena and Tembhurkar [28], who reported that the chloride permeability of freshwater and TWW were classified at 90 days as “very low permeability” and “low permeability”, respectively.

Despite the increase in the chloride permeability observed in TWW concrete in this study and previous studies [27,30], Fig. 8(b) shows that the incorporation of 20 wt% and 35 wt% FA in specimens T0-F20-C0, T100-F20-C0, and T100-F35-C0 decreased the Coulomb charges at 28 days by 43.4%, 55.6%, and 71.7%, respectively, in comparison with their counterparts with no FA. The charges have further decreased at 90 days by 47.3%, 68.1%, and 78.7%, respectively. Furthermore, specimens incorporating FA were classified as “very low permeability”, while

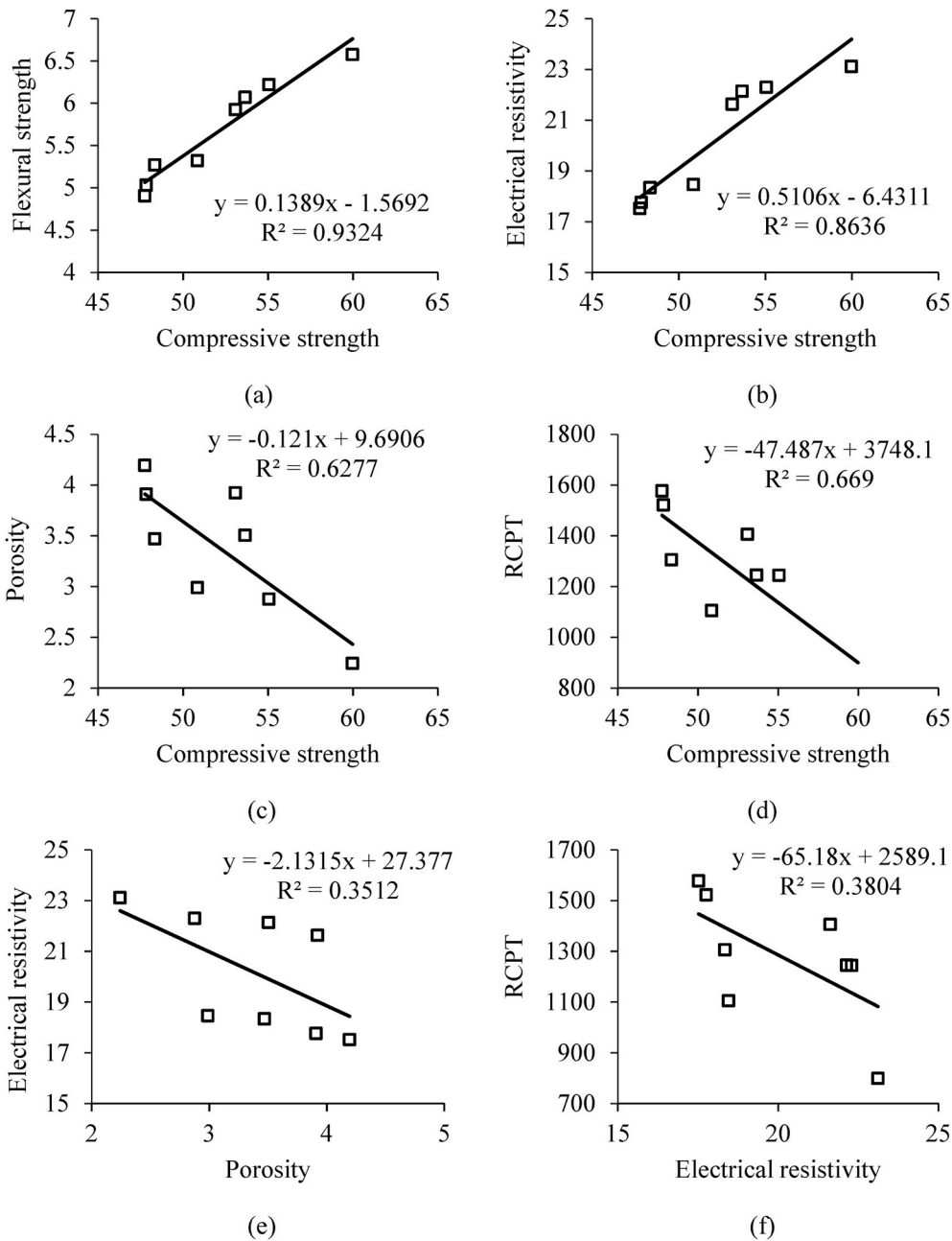


Fig. 12. Linear relationships between the investigated properties of group I.

their counterparts with no FA were classified as “low permeability” as per ASTM C1202-19 standards [77]. This is attributed to the small-size particle of FA, which filled concrete voids and thus produced denser microstructure. The lower charges with FA might also be linked to the chloride binding capacity of the FA, which absorbed and demobilize the chloride ions [35–37].

On the other hand, Fig. 8(c) indicates that adding 3% CN in specimen T0-F0-C3 increased total charges by 18.8% and 39.3% at 28 and 90 days, respectively, owing to the excessive formation of ettringite needles with calcium, which increased concrete pores [54]. However, ettringite formed in specimen T100-F0-C3 has reacted with sulfate ions in TWW and produced monosulphoaluminate hydrate [84]. Thus, Coulomb charges in specimen T100-F0-C3 decreased by 17.4% and 32.4% at 28 and 90 days, respectively, compared to specimen T100-F0-C0. Moreover, incorporating both CN and FA simultaneously in T100-F20-C3 has further decreased the total charges by 23.3% and 49.9%, respectively,

compared to T100-F0-C0. This enhancement is attributed to the addition of FA, which decreased concrete microstructure and demobilized chloride ions. It is worth noting that the lowest chloride penetration was observed in FA concrete made with no CN. These observations agree with the electrical resistivity and porosity test results.

3.3.4. Microstructural analysis

The SEM images for all concrete mixes after 28 days of curing are presented in Fig. 9. It could be observed that regardless of the additive used, freshwater concrete specimens revealed more densified microstructure and homogeneous surface texture than their counterparts with TWW. Fig. 9(a)–(d) shows that mix T0-F0-C0 exhibited a larger amount of portlandite (i.e., a cement hydration product) than TWW concrete mixes, indicating a higher rate of hydration for freshwater specimens. It could also be noticed that gradually incorporating TWW in mixes T25-F0-C0, T50-F0-C0, and T100-F0-C0 has gradually raised concrete

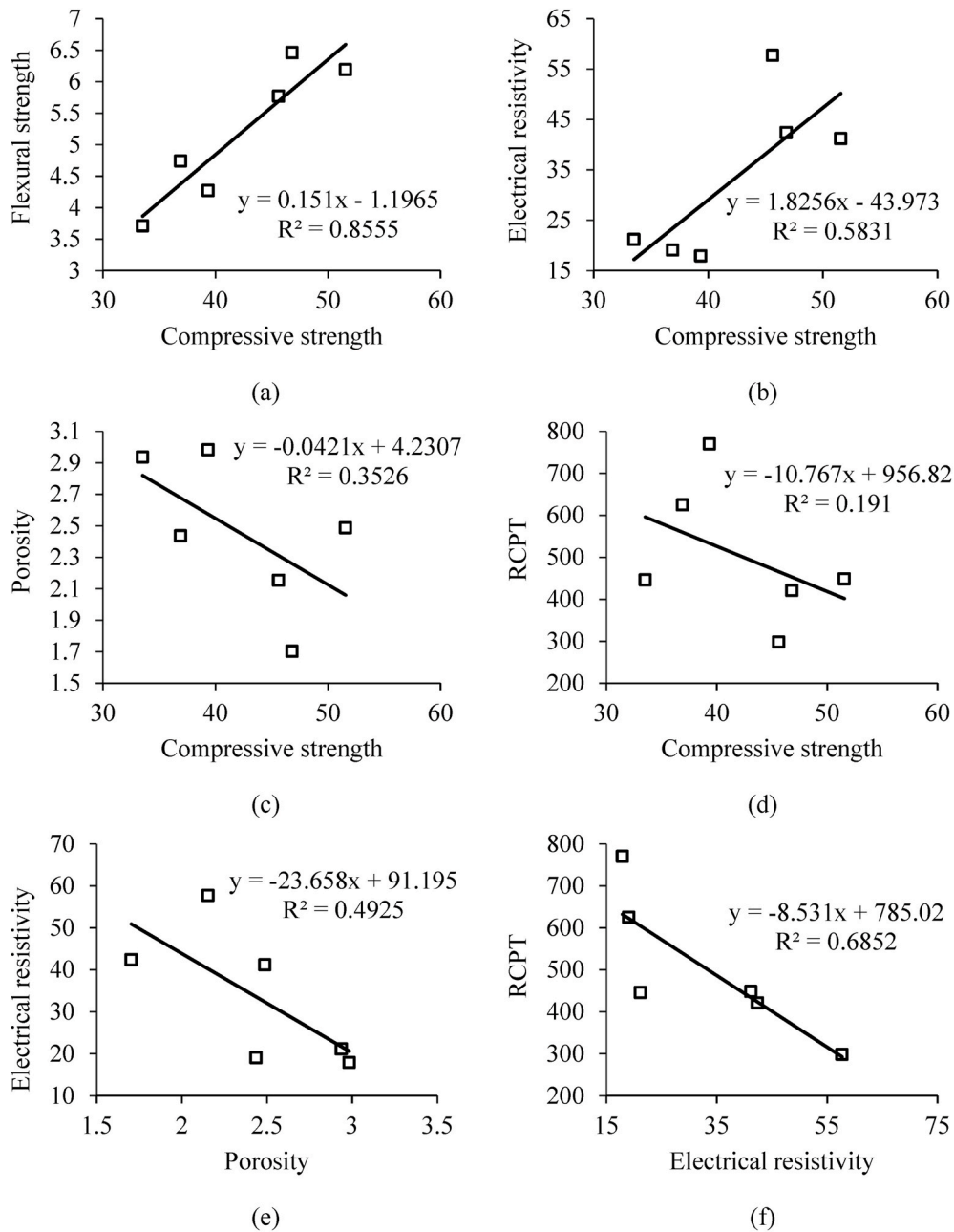


Fig. 13. Linear relationships between the investigated properties of group II.

pores (black color), anhydrous cement (white color), and surface cracks. This is primarily attributed to the presence of dissolved oxygen and suspended solid particles in TWW, which alerted the ITZ layer between cement and aggregates. These observations might explain the drop in the mechanical and durability properties of TWW concrete specimens presented earlier. On the other hand, replacing 20 wt% and 35 wt% OPC with FA in mixes T0-F20-C0, T100-F20-C0, and T100-F35-C0 (Fig. 9(e)–(g)) resulted in a densified cement matrix because of the smaller size particles of FA and the pozzolanic reactions with $\text{Ca}(\text{OH})_2$ [47,49]. These observations might be linked to the superior durability properties obtained for FA concrete specimens. By contrast, Fig. 9(h) shows that adding 3% CN to freshwater concrete specimens excessively formed ettringite needles and thus increased the number of pores. However, adding 3% CN to TWW concrete specimens resulted in a densified microstructure and fewer voids compared to specimens made without CN (Fig. 9(i)). That was due to the presence of sulfate in TWW, which reacted with ettringite and C_3A and produced monosulphoaluminate

hydrate [84]. This might explain why mix T100-F0-C3 reported better mechanical and durability properties than T100-F0-C0. Mix T100-F20-C3, which incorporated both FA and CN, showed approximately similar microstructure to that of T100-F20-C0, but with more ettringite needles (Fig. 9 (j)).

On the other hand, chemical characterizations of all concrete mixes were obtained using EDX microanalysis. As shown in Fig. 10, TWW concrete specimens had no new chemical element formation in comparison with reference concrete. However, the results indicate that calcium intensity in mix T0-F0-C0 was noticeably higher than that of mixes T25-F0-C0, T50-F0-C0, and T100-F0-C0 (Fig. 10(a)–(d)). That was because zinc and phosphate salts in the TWW delayed the hydration of C_3A in TWW concrete mixes [18]. This can explain the slight reduction in the mechanical properties of TWW concrete. Furthermore, silica was found in higher amounts in mixes C0-F20-C0, C100-F20-C0, and C100-F35-C0 compared to their counterparts with no FA (Fig. 10(e)–(g)). This could be attributed to the pozzolanic reactions between FA and

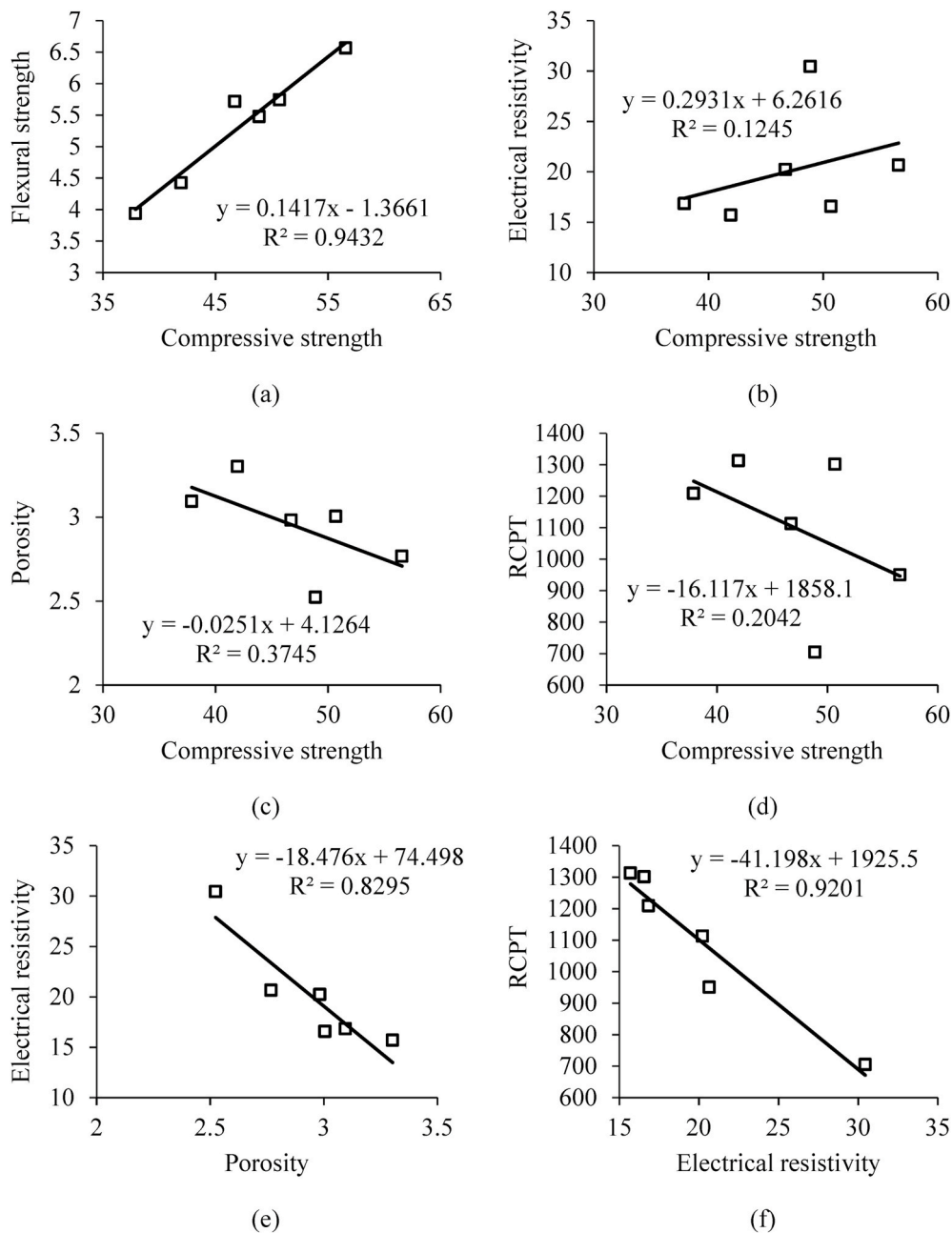


Fig. 14. Linear relationships between the investigated properties of group III.

$\text{Ca}(\text{OH})_2$, which assimilated calcium and converted it to C–S–H gel [47, 49] (i.e., silica content represents the pozzolanic reactions with $\text{Ca}(\text{OH})_2$) [88]. Furthermore, it could be seen that TWW-FA concrete mixes with lower Ca/Si ratios recorded higher compressive strength. This could be seen in mixes C100–F20–C0 and C100–F35–C0, of which they reported Ca/Si ratios of 0.86 and 1.17 and 28-day compressive strength of 36.9 and 33.5 MPa, respectively (see Figs. 4 and 10). The addition of 3% CN in mix T0–F0–C3 resulted in considerably lesser amounts of silica and calcium compared to mix T0–F0–C0 (see Fig. 10 (a) and (h)). This is attributed to the formation of ettringite needles, which consumed the gypsum (i.e., $\text{C}\bar{\text{S}}\text{H}$) [54]. By contrast, Fig. 10(i) shows that mix T100–F0–C3 had higher amounts of silica and calcium than mixes T0–F0–C3 and T100–F0–C0, owing to the formation of calcium monosulphoaluminate hydrate (i.e., $\text{C}_4\text{ASH}_{12}$) [84]. Furthermore, Fig. 10(j) shows that mix T100–F20–C3 reported lower calcium atoms and higher

silica than mix T100–F0–C3 because of the pozzolanic reactions between FA and $\text{Ca}(\text{OH})_2$ [83].

The XRD peaks of all concrete mixes are shown in Fig. 11. The results revealed that TWW had no effect on the chemical compounds of concrete (Fig. 11(a)–(d)). Nevertheless, Fig. 11(e)–(g) shows that mixes T0–F20–C0, T100–F20–C0, and T100–F30–C0 had high intensities of labradorite, indicating the presence of more of C–S–H gel, which resulted from the pozzolanic reactions between FA and $\text{Ca}(\text{OH})_2$. It could also be noticed that mix T0–F0–C3 had higher intensities of portlandite than mixes T100–F0–C3 and T100–F20–C3 (Fig. 11(h)–(j)). This can be linked to the high ettringite needles in mix T0–F0–C3, which was shown in Fig. 9 (h). This might explain the drop in the mechanical and durability properties of mix T0–F0–C3.

3.4. Statistical relationships between concrete properties

The investigated concrete properties were statistically correlated using Pearson correlation with a significance level of 0.05. As the properties were significantly varied among the studied parameters (i.e., TWW, FA, and CN); therefore, concrete mixes were divided into three groups to improve the accuracy of the linear relationships. Groups I, II, and III are related to concrete mixes with TWW, FA, and CN, respectively. The correlation test results are presented in Table 9. In addition, linear relationships between concrete properties were statistically derived for the three groups to predict the mechanical and durability properties without the necessity to perform all tests (Figs. 12–14). For groups I and II, it could be noticed that concrete compressive strength, flexural tensile strength, and electrical resistivity were highly positively correlated with a correlation coefficient (r) ranging from 0.764 to 0.987. However, both compressive and flexural strengths had a low positive correlation with the electrical resistivity for group III ($r = 0.353$), attributable to the formation of high ettringite needles in CN mixes, which, in turn, decreased the durability properties. The same observation could also be seen in the linear relationships between compressive strength and flexural strength (Figs. 12(a), 13(a), and 14(a)) and electrical resistivity (Figs. 12(b), 13(b), and 14(b)), of which the linear relationships of TWW and FA concrete mixes were stronger than those of CN mixes. Despite the differences in the correlation coefficient and determination coefficient (R^2) among the three groups, a positive correlation coefficient indicates that increasing one of these properties increases the other two properties, agreeing well with the experimental results. Furthermore, the mechanical properties in group I were highly negatively correlated with porosity and chloride permeability ($r < -0.710$). This could also be proved by the strong linear relationships between TWW concrete compressive strength, porosity, and chloride permeability (Fig. 12(c) and (d)), of which R^2 was greater than 0.62, suggesting that increasing the compressive strength of TWW concrete improves the durability properties. Moreover, the correlation and linear regression between concrete mechanical properties and porosity and chloride permeability were varied between low to high for groups II and III (see Table 9 and Figs. 13(c) and (d) and 14(c) and (d)). This is attributed to the inclusion of 35% FA in mix T100-F35-C0, which reduced its mechanical characteristics while considerably improved its durability properties compared to mixes T0-F20-C0 and T100-F20-C0, and hence influenced the linearity of the relationship. The fact that CN has a distinct effect on the TWW and freshwater mixtures might explain why group III had low correlations between mechanical and durability properties. It could also be observed that the durability properties expressed moderate to high correlations for the three groups. Furthermore, porosity and electrical resistivity, and electrical resistivity and chloride permeability were shown to have a negative correlation, as shown in Figs. 12(e) and (f), 13(e) and (f), and 14(e) and (f).

4. Conclusions

This study explored the influence of TWW, FA, and CN simultaneously on concrete fresh slump and density, compressive strength, flexural tensile strength, electrical resistivity, porosity, and rapid chloride permeability. Analytical tests, including SEM, EDX and XRD, were also performed to support the experimental results. The main experimental and analytical results are summarized as follows:

1. The use of TWW increased both the initial and final setting time of OPC paste by 20.7% and 29.2%, respectively. Moreover, OPC mortars mixed and cured with TWW exhibited 2%–6% higher compressive strength at 7 days than the reference mortars. On the other hand, TWW showed no effect on concrete fresh slump and density.
2. The use of 25 wt%, 50 wt%, and 100 wt% TWW slightly decreased the compressive and flexural tensile strengths by 5%–12%. Furthermore, the rate of increase of compressive and flexural

strengths with time decreased as the TWW replacement ratio increased.

3. Concrete electrical resistivity for 100% TWW concrete was decreased by 6.5%. Furthermore, the use of 100% TWW increased concrete porosity and Coulomb charges by 27% and 42.7%, respectively, compared to conventional concrete.
4. The incorporation of FA decreased concrete compressive and flexural strengths. However, the durability of FA concrete made with and without TWW has outperformed all other mixes. Moreover, 20 wt% FA concrete with and without TWW was found to be effective in achieving comparable mechanical results to that of the reference mix at later ages.
5. Adding CN in freshwater concrete mixes deteriorated both mechanical and durability properties at all ages, whilst it improved the properties of TWW concrete mixes.
6. SEM images showed that TWW concrete reported more cracks and a higher number of pores than freshwater concrete. Furthermore, concrete with FA reported the most densified cement matrix.
7. EDX microanalysis showed that intensities of silica in FA concrete mixes are higher than their counterparts with no FA. Similar results were also observed by XRD tests, where more labradorite was found in FA mixes.
8. The compressive strength of concrete was positively correlated with flexural strength and electrical resistivity. In addition, the electrical resistivity was negatively correlated with the chloride permeability.

Finally, the current investigation demonstrates the potential of using TWW as a sustainable alternative to freshwater in concrete. However, it should be emphasized that the above conclusions are based on the test results for TWW, FA and CN used in this study. Therefore, more experimental data are required to validate these results. The long-term behavior of TWW concrete is currently under investigation.

CRedit author statement

Abdelrahman Abushanab: Investigation, Formal analysis, Data curation, Software, Original draft preparation, Visualization. **Wael Alnahhal:** Conceptualization, Methodology, Validation, Writing - Review & Editing, Resources Funding acquisition, Supervision Project administration.

Declaration of competing interest

The authors declare that they have no known competing financial interests or personal relationships that could have appeared to influence the work reported in this paper.

Acknowledgment

This publication was made possible by GSRA grant GSRA6-1-0509-19022 from the Qatar National Research Fund (QNRF, a member of Qatar Foundation). The authors would like also to thank the Central Laboratories Unit (CLU) at Qatar University for the scanning electron microscopy and energy-dispersive X-ray microanalysis images. Also, the financial support from Qatar University through grant no. QUST-1-CENG-2021-20 is acknowledged. Open Access funding provided by the Qatar National Library. The findings achieved herein are solely the responsibility of the authors.

References

- [1] E. Aprianti, S. A huge number of artificial waste material can be supplementary cementitious material (SCM) for concrete production – a review part II, *J. Clean. Prod.* 142 (2017) 4178–4194, <https://doi.org/10.1016/j.jclepro.2015.12.115>.
- [2] A. Younis, U. Ebead, P. Suraneni, A. Nanni, Performance of seawater-mixed recycled-aggregate concrete, *J. Mater. Civ. Eng.* 32 (2020) 4019331, [https://doi.org/10.1061/\(ASCE\)MT.1943-5533.0002999](https://doi.org/10.1061/(ASCE)MT.1943-5533.0002999).

- [3] S.A. Miller, A. Horvath, P.J.M. Monteiro, Impacts of booming concrete production on water resources worldwide, *Nat. Sustain.* 1 (2018) 69–76, <https://doi.org/10.1038/s41893-017-0009-5>.
- [4] World Water Assessment Programme (United Nations), *Water: A Shared Responsibility*, United Nations Educational Scientific and Cultural (UNESCO), 2006.
- [5] M. Farhadkhani, M. Nikaeen, G. Yadegarfar, M. Hatamzadeh, H. Pourmohammadbagher, Z. Sahbaei, H.R. Rahmani, Effects of irrigation with secondary treated wastewater on physicochemical and microbial properties of soil and produce safety in a semi-arid area, *Water Res.* 144 (2018) 356–364, <https://doi.org/10.1016/j.watres.2018.07.047>.
- [6] N. Ghaffour, T.M. Missimer, G.L. Amy, Technical review and evaluation of the economics of water desalination: current and future challenges for better water supply sustainability, *Desalination* 309 (2013) 197–207, <https://doi.org/10.1016/j.desal.2012.10.015>.
- [7] M. Elimelech, W.A. Phillip, The future of seawater desalination: energy, technology, and the environment, *Science* 80– (333) (2011) 712 LP–717, <https://doi.org/10.1126/science.1200488>.
- [8] S. Miller, H. Shemer, R. Semiat, Energy and environmental issues in desalination, *Desalination* 366 (2015) 2–8, <https://doi.org/10.1016/j.desal.2014.11.034>.
- [9] G. Asadollahfardi, M. Delnavaz, V. Rashnoiee, N. Ghonabadi, Use of treated domestic wastewater before chlorination to produce and cure concrete, *Construct. Build. Mater.* 105 (2016) 253–261, <https://doi.org/10.1016/j.conbuildmat.2015.12.039>.
- [10] M.F. Arooj, F. Haseeb, A.I. Butt, D.M. Irfan-Ul-Hassan, H. Batool, S. Kibriya, Z. Javed, H. Nawaz, S. Asif, A sustainable approach to reuse of treated domestic wastewater in construction incorporating admixtures, *J. Build. Eng.* 33 (2021) 101616, <https://doi.org/10.1016/j.jobe.2020.101616>.
- [11] K. Meena, S. Luhar, Effect of wastewater on properties of concrete, *J. Build. Eng.* 21 (2019) 106–112, <https://doi.org/10.1016/j.jobe.2018.10.003>.
- [12] N.C. Duarte, A.E. Amaral, B.G. Gomes, G.H. Siqueira, A.L. Tonetti, Water reuse in the production of non-reinforced concrete elements: an alternative for decentralized wastewater management, *J. Water, Sanit. Hyg. Dev.* 9 (2019) 596–600, <https://doi.org/10.2166/washdev.2019.106>.
- [13] ASTM 1602/C1602M – 18, Standard Specification for Mixing Water Used in the Production of Hydraulic Cement Concrete, 2018, <https://doi.org/10.1520/C1602-C1602M-18>.
- [14] Cement Concrete, Aggregates Australia, Chloride resistance of concrete. https://www.ccaa.com.au/imis_prod/documents/Library Documents/CCAA Reports /Report 2009 ChlorideResistance.pdf, 2009.
- [15] BS:EN:1008, Mixing water for concrete: specification for sampling, testing and assessing the suitability of water, including water recovered from processes in the concrete industry as mixing water for concrete, *Br. Stand. Inst.* 2002 (2002).
- [16] J. Tay, W. Yip, Use of reclaimed wastewater for concrete mixing, *J. Environ. Eng.* 113 (1987) 1156–1161, [https://doi.org/10.1061/\(ASCE\)0733-9372\(1987\)113:5\(1156\)](https://doi.org/10.1061/(ASCE)0733-9372(1987)113:5(1156)).
- [17] S. Ahmed, Y. Alhoubi, N. Elmesalami, S. Yehia, F. Abed, Effect of recycled aggregates and treated wastewater on concrete subjected to different exposure conditions, *Construct. Build. Mater.* 266 (2021) 120930, <https://doi.org/10.1016/j.conbuildmat.2020.120930>.
- [18] O.S. Lee, M.R. Salim, M. Ismail, M.I. Ali, Reusing treated effluent in concrete technology, *J. Teknol.* 34 (2001), <https://doi.org/10.11113/jt.v34.648>.
- [19] O.Z. Cebeci, A.M. Saatci, Domestic sewage as mixing water in concrete, *Mater. J.* 86 (1989) 503–506.
- [20] D. Ng, M.G. Shaaban, L. Keong, Effect of impurities in mixing waters on cement/concrete blocks compressive strength, in: *Natl. Semin. Adv. Environ. Control Technol*, Kuala Lumpur Univ. Teknol. Malaysia, 1993, pp. 18–19.
- [21] M. Shaikh, V. Inamdar, Study of utilization of waste water in concrete, *IOSR J. Mech. Civ. Eng.* 13 (2016) 105–108, <https://doi.org/10.9790/1684-130402105108>.
- [22] A.M. Ghrair, O. Al-mashaqbeh, Domestic wastewater reuse in concrete using bench-scale testing and full-scale implementation, *Water* 8 (2016) 366, <https://doi.org/10.3390/w8090366>.
- [23] I. Al-Ghusain, M. Terro, Use of treated wastewater for concrete mixing in Kuwait, *Kuwait J. Sci. Eng.* 30 (2003).
- [24] M. Shekarchi, M. Yazdian, N. Mehrdadi, Use of biologically treated domestic waste water in concrete, *Kuwait J. Sci. Eng.* 39 (2012) 97–111.
- [25] A.H. Noruzman, B. Muhammad, M. Ismail, Z. Abdul-Majid, Characteristics of treated effluents and their potential applications for producing concrete, *J. Environ. Manag.* 110 (2012) 27–32, <https://doi.org/10.1016/j.jenvman.2012.05.019>.
- [26] ASTM C94/C94M – 20, Standard Specification for Ready-Mixed Concrete, 2020, https://doi.org/10.1520/C0094_C0094M-20.
- [27] P.R.M. Rao, S.M.K. Moinuddin, P. Jagadeesh, Effect of treated waste water on the properties of hardened concrete, *Int. J. Chem. Sci.* 12 (2014) 155–162.
- [28] S. Saxena, A.R. Tembhurkar, Impact of use of steel slag as coarse aggregate and wastewater on fresh and hardened properties of concrete, *Construct. Build. Mater.* 165 (2018) 126–137, <https://doi.org/10.1016/j.conbuildmat.2018.01.030>.
- [29] F.S. Peighambarzadeh, G. Asadollahfardi, J. Akbaridoost, The effects of using treated wastewater on the fracture toughness of the concrete, *Aust. J. Civ. Eng.* 18 (2020) 56–64, <https://doi.org/10.1080/14488353.2020.1712933>.
- [30] M.S. Hassani, G. Asadollahfardi, S.F. Saghravani, S. Jafari, F.S. Peighambarzadeh, The difference in chloride ion diffusion coefficient of concrete made with drinking water and wastewater, *Construct. Build. Mater.* 231 (2020) 117182, <https://doi.org/10.1016/j.conbuildmat.2019.117182>.
- [31] C. Magro, J.M. Paz-Garcia, L.M. Ottosen, E.P. Mateus, A.B. Ribeiro, Sustainability of construction materials: electro-dialytic technology as a tool for mortars production, *J. Hazard Mater.* 363 (2019) 421–427, <https://doi.org/10.1016/j.jhazmat.2018.10.010>.
- [32] R. Kurda, J. de Brito, J.D. Silvestre, Combined economic and mechanical performance optimization of recycled aggregate concrete with high volume of fly ash, *Appl. Sci.* 8 (2018) 1189, <https://doi.org/10.3390/app8071189>.
- [33] B. Ali, L.A. Qureshi, Influence of glass fibers on mechanical and durability performance of concrete with recycled aggregates, *Construct. Build. Mater.* 228 (2019) 116783, <https://doi.org/10.1016/j.conbuildmat.2019.116783>.
- [34] R. Kurad, J.D. Silvestre, J. de Brito, H. Ahmed, Effect of incorporation of high volume of recycled concrete aggregates and fly ash on the strength and global warming potential of concrete, *J. Clean. Prod.* 166 (2017) 485–502, <https://doi.org/10.1016/j.jclepro.2017.07.236>.
- [35] T. Cheewaket, C. Jaturapitakkul, W. Chalee, Long term performance of chloride binding capacity in fly ash concrete in a marine environment, *Construct. Build. Mater.* 24 (2010) 1352–1357, <https://doi.org/10.1016/j.conbuildmat.2009.12.039>.
- [36] B. Ma, X. Liu, H. Tan, T. Zhang, J. Mei, H. Qi, W. Jiang, F. Zou, Utilization of pretreated fly ash to enhance the chloride binding capacity of cement-based material, *Construct. Build. Mater.* 175 (2018) 726–734, <https://doi.org/10.1016/j.conbuildmat.2018.04.178>.
- [37] A. Noushini, A. Castel, J. Aldred, A. Rawal, Chloride diffusion resistance and chloride binding capacity of fly ash-based geopolymer concrete, *Cement Concr. Compos.* 105 (2020) 103290, <https://doi.org/10.1016/j.cemconcomp.2019.04.006>.
- [38] A. Al-Hamrani, M. Kukukvar, W. Alnahhal, E. Mahdi, N.C. Onat, Green concrete for a circular economy: a review on sustainability, durability, and structural properties, *Materials* 14 (2021), <https://doi.org/10.3390/ma14020351>.
- [39] M.V.A. Florea, H.J.H. Brouwers, Modelling of chloride binding related to hydration products in slag-blended cements, *Construct. Build. Mater.* 64 (2014) 421–430, <https://doi.org/10.1016/j.conbuildmat.2014.04.038>.
- [40] R. Luo, Y. Cai, C. Wang, X. Huang, Study of chloride binding and diffusion in GGBS concrete, *Cement Concr. Res.* 33 (2003) 1–7, [https://doi.org/10.1016/S0008-8846\(02\)00712-3](https://doi.org/10.1016/S0008-8846(02)00712-3).
- [41] C. Arya, Y. Xu, Effect of cement type on chloride binding and corrosion of steel in concrete, *Cement Concr. Res.* 25 (1995) 893–902, [https://doi.org/10.1016/0008-8846\(95\)00080-V](https://doi.org/10.1016/0008-8846(95)00080-V).
- [42] Z. Shi, M.R. Geiker, K. De Weerd, T.A. Østnor, B. Lothenbach, F. Winnefeld, J. Skibsted, Role of calcium on chloride binding in hydrated Portland cement–metakaolin–limestone blends, *Cement Concr. Res.* 95 (2017) 205–216, <https://doi.org/10.1016/j.cemconres.2017.02.003>.
- [43] G.M. Wang, Y. Kong, Z.H. Shui, Q. Li, J.L. Han, Experimental investigation on chloride diffusion and binding in concrete containing metakaolin, *Corrosion Eng. Sci. Technol.* 49 (2014) 282–286, <https://doi.org/10.1179/1743278213Y.0000000134>.
- [44] Y. Elakneswaran, T. Nawa, K. Kurumisawa, Electrokinetic potential of hydrated cement in relation to adsorption of chlorides, *Cement Concr. Res.* 39 (2009) 340–344, <https://doi.org/10.1016/j.cemconres.2009.01.006>.
- [45] M. Balonis, B. Lothenbach, G. Le Saout, F.P. Glasser, Impact of chloride on the mineralogy of hydrated Portland cement systems, *Cement Concr. Res.* 40 (2010) 1009–1022, <https://doi.org/10.1016/j.cemconres.2010.03.002>.
- [46] A. Mesbah, M. François, C. Cau-dit-Coumes, F. Frizon, Y. Filinchuk, F. Leroux, J. Ravaut, G. Renaudin, Crystal structure of Kuzel’s salt $3\text{CaO}\cdot\text{Al}_2\text{O}_3\cdot 1/2\text{CaSO}_4\cdot 1/2\text{CaCl}_2\cdot 11\text{H}_2\text{O}$ determined by synchrotron powder diffraction, *Cem. Concr. Res.* 41 (2011) 504–509, <https://doi.org/10.1016/j.cemconres.2011.01.015>.
- [47] M.D.A. Thomas, R.D. Hooton, A. Scott, H. Zibara, The effect of supplementary cementitious materials on chloride binding in hardened cement paste, *Cement Concr. Res.* 42 (2012) 1–7, <https://doi.org/10.1016/j.cemconres.2011.01.001>.
- [48] S.C. Kou, C.S. Poon, D. Chan, Influence of fly ash as cement replacement on the properties of recycled aggregate concrete, *J. Mater. Civ. Eng.* 19 (2007) 709–717, [https://doi.org/10.1061/\(ASCE\)0899-1561\(2007\)19:9\(709\)](https://doi.org/10.1061/(ASCE)0899-1561(2007)19:9(709)).
- [49] S.C. Kou, C.S. Poon, D. Chan, Influence of fly ash as a cement addition on the hardened properties of recycled aggregate concrete, *Mater. Struct.* 41 (2008) 1191–1201, <https://doi.org/10.1617/s11527-007-9317-y>.
- [50] M.J. McCarthy, R.K. Dhir, Development of high volume fly ash cements for use in concrete construction, *Fuel* 84 (2005) 1423–1432, <https://doi.org/10.1016/j.fuel.2004.08.029>.
- [51] F.A. Sabet, N.A. Libre, M. Shekarchi, Mechanical and durability properties of self consolidating high performance concrete incorporating natural zeolite, silica fume and fly ash, *Construct. Build. Mater.* 44 (2013) 175–184, <https://doi.org/10.1016/j.conbuildmat.2013.02.069>.
- [52] D. Wang, X. Zhou, Y. Meng, Z. Chen, Durability of concrete containing fly ash and silica fume against combined freezing–thawing and sulfate attack, *Construct. Build. Mater.* 147 (2017) 398–406, <https://doi.org/10.1016/j.conbuildmat.2017.04.172>.
- [53] H.Z. Lopez-Calvo, P. Montes-García, T.W. Bremner, M.D.A. Thomas, V.G. Jiménez-Quero, Compressive strength of HPC containing CNI and fly ash after long-term exposure to a marine environment, *Cement Concr. Compos.* 34 (2012) 110–118, <https://doi.org/10.1016/j.cemconcomp.2011.08.007>.
- [54] Z. Li, B. Ma, J. Peng, M. Qi, The microstructure and sulfate resistance mechanism of high-performance concrete containing CNI, *Cement Concr. Compos.* 22 (2000) 369–377, [https://doi.org/10.1016/S0958-9465\(00\)00028-7](https://doi.org/10.1016/S0958-9465(00)00028-7).
- [55] K.Y. Ann, H.S. Jung, H.S. Kim, S.S. Kim, H.Y. Moon, Effect of calcium nitrite-based corrosion inhibitor in preventing corrosion of embedded steel in concrete, *Cement Concr. Res.* 36 (2006) 530–535, <https://doi.org/10.1016/j.cemconres.2005.09.003>.

- [56] J. Milla, M.M. Hassan, T. Rupnow, M. Alansari, G. Arce, Effect of self-healing calcium nitrate microcapsules on concrete properties, *Transp. Res. Rec. J. Transp. Res. Board.* 2577 (2016) 69–77, <https://doi.org/10.3141/2577-09>.
- [57] N.S. Berke, M.C. Hicks, Predicting long-term durability of steel reinforced concrete with calcium nitrite corrosion inhibitor, *Cement Concr. Compos.* 26 (2004) 191–198, [https://doi.org/10.1016/S0958-9465\(03\)00038-6](https://doi.org/10.1016/S0958-9465(03)00038-6).
- [58] K.K. Sideris, A.E. Savva, Durability of mixtures containing calcium nitrite based corrosion inhibitor, *Cement Concr. Compos.* 27 (2005) 277–287, <https://doi.org/10.1016/j.cemconcomp.2004.02.016>.
- [59] ASTM C150/C150M – 20, Standard Specification for Portland Cement, 2020, https://doi.org/10.1520/C0150_C0150M-20.
- [60] ASTM C188 – 17, Standard Test Method for Density of Hydraulic Cement, 2017, <https://doi.org/10.1520/C0188-17>.
- [61] ASTM C311/C311M – 18, Standard Test Methods for Sampling and Testing Fly Ash or Natural Pozzolans for Use in Portland-Cement Concrete, 2018, https://doi.org/10.1520/C0311_C0311M-18.
- [62] B.D. Wheeler, Chemical analysis of Portland cement by energy dispersive X-ray fluorescence, *Cem. Concr. Aggregates* 5 (1983) 123–127, <https://doi.org/10.1520/CCA10262J>.
- [63] ASTM C618 – 19, Standard specification for coal fly ash and raw or calcined natural pozzolan for use in concrete. <https://doi.org/10.1520/C0618-19>, 2019.
- [64] ASTM C33/C33M – 18, Standard specification for concrete aggregates. https://doi.org/10.1520/C0033_C0033M-18, 2018.
- [65] World Health Organization, *Guidelines for drinking-water quality*, Geneva, Switzerland, 2011.
- [66] American Public Health Association, *Standard Methods for the Examination of Water and Wastewater*, 22st ed., American Public Health Association, Washington DC, USA, 2012. <https://books.google.com.qa/books?id=dd2juAAACAAJ>.
- [67] QCS, *Qatar General Organization for Standards and Metrology*, Qatar, 2014.
- [68] ASTM C192/C192M – 19, Standard practice for making and curing concrete test specimens in the laboratory. https://doi.org/10.1520/C0192_C0192M-19, 2019.
- [69] ASTM C191 – 19, Standard test methods for time of setting of hydraulic cement by vicat needle. <https://doi.org/10.1520/C0191-19>, 2019.
- [70] ASTM C109/C109M – 20b, Standard test method for compressive strength of hydraulic cement mortars (Using 2-in. Or [50 mm] cube specimens). https://doi.org/10.1520/C0109_C0109M-20B, 2020.
- [71] ASTM C143/C143M-15a, Standard Test Method for Slump of Hydraulic-Cement Concrete, 2015, pp. 15–18, https://doi.org/10.1520/C0143_C0143M-15A.
- [72] ASTM C138/C138M – 17a, Standard test method for density (unit weight), yield, and air content (gravimetric) of concrete. https://doi.org/10.1520/C0138_C0138M-17A, 2017.
- [73] ASTM C39/C39M-20, Standard Test Method for Compressive Strength of Cylindrical Concrete Specimens, 2020, pp. 1–8, https://doi.org/10.1520/C0039_C0039M-20.
- [74] ASTM C78/C78M – 18, Standard Test Method for Flexural Strength of Concrete (Using Simple Beam with Third-Point Loading), 2018, https://doi.org/10.1520/C0078_C0078M-18.
- [75] AASHTO TP 95, *Standard Method of Test for Surface Resistivity Indication of Concrete's Ability to Resist Chloride Ion Penetration*, American Association of State Highway and Transportation Officials, Washington, DC, 2011.
- [76] ASTM C1754/C1754M-12, Standard Test Method for Density and Void Content of Hardened Pervious Concrete, 2012.
- [77] ASTM C1202-19, Standard Test Method for Electrical Indication of Concrete's Ability to Resist Chloride Ion Penetration1, 2019, <https://doi.org/10.1520/C1202-19>.
- [78] ASTM C1723 – 16, Standard Guide for Examination of Hardened Concrete Using Scanning Electron Microscopy, 2016, <https://doi.org/10.1520/C1723-16>.
- [79] A.M. Neville, *Properties of Concrete*, Longman London, 1995.
- [80] M.L. Berndt, Properties of sustainable concrete containing fly ash, slag and recycled concrete aggregate, *Construct. Build. Mater.* 23 (2009) 2606–2613, <https://doi.org/10.1016/j.conbuildmat.2009.02.011>.
- [81] M.A. Blankson, S. Erdem, Comparison of the effect of organic and inorganic corrosion inhibitors on the rheology of self-compacting concrete, *Construct. Build. Mater.* 77 (2015) 59–65, <https://doi.org/10.1016/j.conbuildmat.2014.12.032>.
- [82] X. Li, L. O'Moore, S. Wilkie, Y. Song, J. Wei, P.L. Bond, Z. Yuan, L. Hanzic, G. Jiang, Nitrite admixed concrete for wastewater structures: mechanical properties, leaching behavior and biofilm development, *Construct. Build. Mater.* 233 (2020) 117341, <https://doi.org/10.1016/j.conbuildmat.2019.117341>.
- [83] D.K. Panesar, 3 - supplementary cementing materials, in: B.T.-D. S (Ed.), *In the F. And R of C. (Second E. Mindess (Ed.), Woodhead Publ. Ser. Civ. Struct. Eng., Woodhead Publishing*, 2019, pp. 55–85, <https://doi.org/10.1016/B978-0-08-102616-8.00003-4>.
- [84] K. Pimraksa, P. Chindaprasit, 14 - sulfoaluminate cement-based concrete, in: F. Pacheco-Torgal, R.E. Melchers, X. Shi, N. De Belie, K. Van Tittelboom, E.-E. R. ABT, R. of, C.I. Sáez (Eds.), *Woodhead Publ. Ser. Civ. Struct. Eng., Woodhead Publishing*, 2018, pp. 355–385, <https://doi.org/10.1016/B978-0-08-102181-1.00014-9>.
- [85] Y. Kocak, S. Nas, The effect of using fly ash on the strength and hydration characteristics of blended cements, *Construct. Build. Mater.* 73 (2014) 25–32, <https://doi.org/10.1016/j.conbuildmat.2014.09.048>.
- [86] R. Kurda, J. de Brito, J.D. Silvestre, Water absorption and electrical resistivity of concrete with recycled concrete aggregates and fly ash, *Cement Concr. Compos.* 95 (2019) 169–182, <https://doi.org/10.1016/j.cemconcomp.2018.10.004>.
- [87] Q. Wang, D. Wang, H. Chen, The role of fly ash microsphere in the microstructure and macroscopic properties of high-strength concrete, *Cement Concr. Compos.* 83 (2017) 125–137, <https://doi.org/10.1016/j.cemconcomp.2017.07.021>.
- [88] V. Kannan, K. Ganesan, Chloride and chemical resistance of self compacting concrete containing rice husk ash and metakaolin, *Construct. Build. Mater.* 51 (2014) 225–234, <https://doi.org/10.1016/j.conbuildmat.2013.10.050>.